AIAA Propulsion and Energy Forum
19-22 August 2019, Indianapolis, IN
AIAA Propulsion and Energy 2019 Forum

10.2514/6.2019-3868

Application of dynamic zone flamelet model to a GH_2/GO_2 rocket combustor

Wei Yao[1] and Bo Li[2]
Key Laboratory of High-Temperature Gas Dynamics, Institute of Mechanics, CAS, Beijing 100190, China
School of Engineering Science, University of Chinese Academy of Science, Beijing 100049, China

A dynamic zone flamelet model is proposed and validated in this study. The model divides the whole computational domain into different zones and uses a local flamelet to describe the chemistry status within each zone. The zone division constantly updates with the time-variant mixture fraction fields. Each zone is in irregular shape and contains a random number of CFD cells. The flamelet evolution equation due to convective transport, molecular diffusion, and chemical reactions is derived through redefining the conditional average within each zone. In highly compressible supersonic flows, the density, temperature, and velocity do not correlate with the mixture fraction any more; thus only the species mass fraction in each flamelet is used. The flamelet temperature equation is not solved, but a computationally-efficient statistical method is used for the conditional temperature, which then determines the reaction progress. The DZFM is then applied to a GH_2/GO_2 rocket combustor based on an Improved Delayed Detached Eddy Simulation (IDDES) framework and a total of 20,557 flamelet zones. The predicted wall heat flux, mean temperature and mean hydrogen concentration are generally comparable with the available experimental measurement and the previous predictions in the literature. The evolution of flamelet variables with the axial height and the time shows that the current model has the capability of characterizing the transient chemistry status, which would especially useful for unsteady combustion modeling by large eddy simulation.

Keywords: dynamic zone flamelet model, rocket combustor, Large Eddy Simulation (LES), GH_2/GO_2, turbulence-chemistry interaction

I. Introduction

An intricate modeling of the turbulence-chemistry interaction (TCI) in engine combustion is difficult because it varies both spatially and temporally. To accurately resolving the unsteady flow, mixing and combustion processes as well as the related flow structures in engine combustors, LES (Large Eddy Simulation) or DNS (Direct Numerical Simulation) based high-resolution and of coarse computationally expansive modeling is usually required. To alleviate the huge computational cost, a prior thing is to speed up the solving of combustion chemistry. Different strategies [1, 2], such as DAC (Dynamic Adaptive Chemistry)[3-6], ISAT (In Situ Adaptive Tabulation) [7, 8], CCM (Chemistry Coordinate Mapping) [9], ANN (Artificial Neural Network) [10-13], and GPU acceleration [14] are adopted to reduce the direct integration (DI) time of stiff chemistry system itself. In addition to those direct acceleration methods, another brilliant idea is to extract the chemistry solving from the flow modeling by using one conserved scalar i.e., mixture fraction together with some other status variables (e.g., scalar dissipation rate, progress variable, and flame front location), i.e., the flamelet concept. In flamelet model (FM) [15], by decoupling the chemistry solving in three-dimensional (3D) space into a virtual one- (1D) or two-dimensional (2D) space coordinated by mixture fraction and status variable, detailed mechanisms with multiple species and stiff reactions can be economically employed in modeling full-scale combustors. Thus the model is extraordinary faster than finite-rate combustion models, e.g., PaSR [16, 17], EDC [18, 19], which not only solve chemistry in multi-dimensional physical space but also transport all the species involved in the kinetic mechanism(s). The applicability of flamelet model generally assumes faster chemistry than turbulent stirring, i.e., thin reaction zone, so that the reactive scalar Y can be related to the mixture fraction ξ and status variable (usually denoted by scalar dissipation rate χ) as $Y = Y(\xi, \chi)$ in the whole flowfield. However, flamelet based models are theoretically inapplicable to the slow chemistry zones.

[1] Associate Professor, Institute of Mechanics (CAS), weiyao@imech.ac.cn, AIAA member (Corresponding author).
[2] PHD student, Institute of Mechanics (CAS), libo2@imech.ac.cn.

For combustion in anisotropic turbulence, which is the case in most jet-fueled combustors, statistical homogeneity of Y versus ξ cannot be assumed. Thus representing the combustion chemistry of a whole flowfield by a single flamelet is not accurate anymore, because the scalars may deviate significantly from the flamelet status. Instead, using the concept of local flamelets, or zone based conditioned variables, for different flow regions bearing different turbulence-chemistry interaction modes may be a more reliable solution, as long as the local statistical homogeneity can be assumed. A concept of zone flamelet model (ZFM) which divides the whole flow field into a set of irregular-shape zones has been proposed in [20] and successfully applied to model a supersonic combustor.

Such a concept of zone-based flamelet or conditioned variables has been implied in the practice of Conditional Moment Closure (CMC) modelings by dividing the flow fields into several CMC zones [21]. However, in previous CMC implements, the CMC zone division is fixed at the beginning and will not adapt to the evolution of flow fields. In many transient problems, such as the ignition/extinction [22-28], the conditional averages show large spatial variations and the local statistical homogeneity varies from time to time. In this study, a dynamic zone flamelet model is developed from the previous static zone flamelet model [20] through adapts the zone division with the time-variant mixture fraction fields. Such a concept of zone flamelet modeling based on dynamic zone division is developed to allow a better local statistical homogeneity and to diminish the redistribution effect of conditional variances. The flamelet equation in a zone conserved form is derived to describe the evolution of conditional variables in an irregular zone containing a random number of CFD (Computational Fluid Dynamics) cells. This study also validates this dynamic zone flamelet model (DZFM) in the modeling of a GH_2/GO_2 rocket combustor.

II. Formulation of dynamic zone flamelet model (DZFM)

In dynamic zone flamelet model, the species are solved in a four-dimensional space, i.e., the physical space and the mixture fraction space, but a great computational cost can still be saved because the zone division in physical space is much coarser than the flow simulation mesh. As the zone shrinks, the stochastic variation deviating from the conditional variables diminishes, and thus the assumption of small conditional fluctuations model is then established. Unlike the generic flamelet model, the conditional variables in each zone are not isolated. Across the zone boundaries, the flamelet exchange information with their neighbor zones through a flux-conserved manner, thus the conditional variables can be transport from upstream to downstream in a flowing manner.

The instantaneous equations for mixture fraction ξ and the species mass fraction Y_i are given by,

$$\rho\frac{\partial\xi}{\partial t}+\rho\vec{U}\cdot\nabla\xi=\nabla\cdot(\rho D\nabla\xi) \tag{1}$$

$$\rho\frac{\partial Y_i}{\partial t}+\rho\vec{U}\cdot\nabla Y_i=\nabla\cdot(\rho D\nabla Y_i)+\rho W_i \tag{2}$$

with ρ is the density, $\vec{U}$ is the velocity vector, D represents the diffusivity, and W_i denotes the reaction rate with unit s^{-1}. Here for simplicity, a unity Liews number is assumed. Using the concept of local representative flamelet Q_i, the instantaneous mass fraction is defined as

$$Y_i(x,t)=Q_i(\eta=\xi(x,t),x\in zone,t)+Q_i'(x,t) \tag{3}$$

where η is the sampling variable in mixture fraction space, x represents the physical coordinate, Q_i' represents the deviation of instantaneous value from the conditional averaged value at $\eta=\xi$. Q_i is defined as the conditional average of $Y_i(x,t)$ at $\xi(x,t)=\eta$ with the zone, i.e., $Q_i=\langle Y_i|\xi(x,t)=\eta,x\in zone\rangle$. Thus $\langle Q_i'|\eta,x\in zone\rangle=0$, and obviously the zone-averaged $\langle Q_i'\rangle_{zone}=\int\langle Q_i'|\eta,x\in zone\rangle P(\eta)\,d\eta=0$, with $P(\eta)$ the probability density function (PDF) describing the distribution of instantaneous ξ within the zone. As the zone shrinks, the number of sampling data points reduces, then Q_i approaches Y_i and $Q_i'\to 0$. Here, conditional density-weighted filtering is not used, because the density fluctuation or even discontinuity of density due to compressibility in supersonic flows [29] will deteriorate the correlation between density-weight variables with the mixture fraction.

Substitute the differentiation of Eq. (3) into Eq. (2), it arrives,

$$\rho\frac{\partial Q_i}{\partial t}+\rho\vec{U}\cdot\nabla Q_i-\rho D(\nabla\xi)^2\frac{\partial^2 Q_i}{\partial\eta^2}+\frac{\partial Q_i}{\partial\eta}\left(\rho\frac{\partial\xi}{\partial t}+\rho\vec{U}\cdot\nabla\xi-\nabla\cdot(\rho D\nabla\xi)\right)$$

$$+\left(\rho\frac{\partial Q_i'}{\partial t}+\rho\vec{U}\cdot\nabla Q_i'-\nabla\cdot(\rho D\nabla Q_i')\right)-\rho D\nabla\xi\cdot\nabla\left(\frac{\partial Q_i}{\partial\eta}\right)-\rho D\nabla^2 Q_i=\rho W_i \tag{4}$$

Substituting Eq. (1) into Eq. (4), and taking the average of Eq. (4) on condition that 1) $\xi(x,t)=\eta$ and 2) within the zone $x\in zone$, it yields the final governing equation for Q_i as,

$$\rho_\eta\frac{\partial Q_i}{\partial t}+\left\langle\rho\vec{U}\middle|\eta\right\rangle_{zone}\cdot\nabla Q_i+E_{ZFM}=\rho_\eta\langle\chi|\eta\rangle_{zone}\frac{\partial^2 Q_i}{\partial\eta^2}+\rho_\eta\langle W_i|\eta\rangle \tag{5}$$

$$\text{with}\quad E_{ZFM}=\left\langle\underbrace{\partial Q_i'/\partial t+\vec{U}\cdot\nabla Q_i'-D\nabla^2 Q_i'}_{e_Y}\middle|\eta\right\rangle_{zone}-\left\langle\rho D\nabla\xi\cdot\nabla\left(\frac{\partial Q_i}{\partial\eta}\right)\middle|\eta\right\rangle_{zone}-\langle\nabla\cdot(\rho D\nabla Q_i)|\eta\rangle_{zone} \tag{6}$$

and χ is the scalar dissipation rate defined as $\chi=D(\nabla\xi)^2$, $\rho_\eta=\langle\rho|\eta\rangle$. Here the conditional averages are taken over each zone, denoted by adding a subscript "zone", and e_Y is used to denote the three conditional fluctuation terms for brief. The second term on the LHS in Eq.(5) represents the convective transport of conditional variables or local flamelet in a flow manner among neighbor zones, the first term on the RHS represents molecular mixing or diffusion in mixture fraction space, whose magnitude is determined by the conditional scalar dissipation rate. The conditional scalar dissipation rate $\langle\chi|\eta\rangle$ is modeled by amplitude mapping closure (AMC) model [30] for its simplicity, since no large difference was observed among AMC [30], Girimaji [31] and PDF integration [32] models for conditional scalar dissipation rate [33]. The last term on the RHS represents the change of conditional or flamelet variables due to the local chemical reactions in the zone. Eq. (5) describes the evolution of conditional variables or local flamelet within a zone due to convective transport, molecular diffusion and local chemistry, thus can also be named as zone flamelet. The generic FM can be considered as a special zone flamelet model taking the whole computational domain as a single zone.

All spatial gradient of Q_i is zero within the zone except on the zone boundary, thus it arrives,

$$\left\langle\rho\vec{U}\middle|\eta\right\rangle_{zone}\cdot\nabla Q_i=\frac{\oiint_{zone\ boundary}\left\langle\rho\vec{U}\middle|\eta\right\rangle\cdot\nabla Q_i}{\oiint_{zone\ boundary}\left\langle\rho\vec{U}\middle|\eta\right\rangle} \tag{7}$$

which is essentially equivalent to the Gauss's flux theorem but conveniently expresses the exchange flux of conditional variables among neighbor zones with irregular shapes. Here, it is assumed that both the density and velocity distributions have weak dependence with the mixture fraction distribution in supersonic flows, but largely influenced by the flow compressibility and discontinuities, thus $\rho_\eta=\rho$ and $\left\langle\vec{U}\middle|\eta\right\rangle=\vec{U}$. Following the analysis in [34], for high-Re flows, $\langle\rho D\nabla\xi\cdot\nabla(\partial Q_i/\partial\eta)|\eta\rangle_{zone}\sim\rho D\xi D^{-1/2}\cdot Q_i\sim D^{1/2}\sim Re^{-1/2}$, and $\langle\nabla\cdot(\rho D\nabla Q_i)|\eta\rangle_{zone}\sim\rho D\cdot Q_i\sim Re^{-1}$ thus can both be neglected in supersonic flows typically with $Re>10^5$.

Using the same closure strategy as in the generic CMC,

$$\int\langle e_Y|\eta\rangle_{zone}P(\eta)d\eta=\langle e_Y\rangle_{zone}=\rho\,\partial\langle Q_i'\rangle_{zone}/\partial t+\rho\vec{U}\cdot\nabla\langle Q_i'\rangle_{zone}-\nabla\cdot\langle\rho D\nabla Q_i'\rangle_{zone}=0 \tag{8}$$

In Eq. (8) the assumption of $\left\langle\vec{U}\middle|\eta\right\rangle=\vec{U}$ is also used to neglect the conditional fluctuations of velocity. From Eq. (8), it seems that the effect of the first three terms in the parenthesis in Eq. (6) is to redistribute Q_i over the mixture fraction space for each zone. As stated by Bilger [35], "if the conditional averages of fluctuations are positive over some range of η, they must be negative over other ranges of η to compensate". Proper evaluation of the redistribution effect of these terms awaits the availability of experimental and DNS data. The general hypothesis in CMC [34] is to neglect the redistribution effect in the η space compared with other terms in the balance, especially when $Re\to\infty$ the small turbulent scales and large scales can be assumed decoupled thus $\langle e_Y|\eta\rangle=\langle e_Y\rangle$ [36]. However, a fine enough zone division in the η space may help to alleviate such a redistribution effect. In this study, the zone is divided in accordance with the η-space discretization based on the quasi-mean mixture fraction field. Here, the quasi-mean mixture fraction is used instead of the instantaneous mixture fraction to avoid the complex interpretation of Lagrangian-type derivative in a moving frame of reference. The quasi-mixture fraction is averaged over a short time window e.g., 1 FTT (flow through time), to reflect a quasi-steady mixture fraction distribution that characterizes the historic integration of local

mixing statuses. The instantaneous mixture fraction in each zone can be considered to correspond to a single η space or a narrow mixture fraction region around it. It is then reasonable to assume that the PDF distribution with each zone shrinks to a Dirac delta function centered on $\eta = \xi$, i.e. $\int \langle e_Y|\eta\rangle_{zone}\, \delta(\eta = \xi) d\eta = \langle e_Y|\eta = \xi\rangle_{zone} = 0$. Thereby, the conditional variance terms can be avoided to close Eq. (5) through a proper zone division based on the mean mixture fraction field. Because the zone division dynamically adapts to the variation of mean mixture fraction field, such an approach is called dynamic zone conditional moment closure.

Eq. (5) is solved by Operator Splitting (OS) method. Firstly, a finite volume method is used to solve the convective part because the flamelet zone can be irregular in geometric shape and contains a random number of CFD cells. The transient term and convection term are integrated over a control volume and the transient PDE in integral form is linearized as follows,

$$\frac{\rho^{n+1}Q_i^{n+1}-\rho^n Q_i^n}{\Delta t} + \frac{\Sigma_f \vec{S}_f \cdot (\rho \vec{U} Q_i^n)_f^n}{\Delta V} = 0 \tag{9}$$

where n and n+1 represents the current and next-step values, f represents boundary faces, $\vec{S}_f$ is the boundary face area vector. Unlike the common practice of discarding the conditional density term in the generic CMC [34, 37], the conditional density ρ_η ($\approx \rho$) is retained to ensure a mass conservation when across the zones. Actually, the conditional density is defined for each zone and varies across the zones, thus cannot be simply discarded as the treatment in a incompressible flow. In determining the face values of Q_i^n, a simple upwind scheme is used. Secondly, the diffusion in mixture fraction space is solved by finite difference method to smooth any peaks in the Q_i distribution,

$$\frac{\partial Q_i}{\partial t} = \langle \chi|\eta\rangle \frac{\partial Q_i}{\partial \xi^2} \tag{10}$$

where $\langle \chi|\eta\rangle$ is modeled by amplitude mapping closure (AMC) model [30], the mean scalar dissipation rate $\tilde{\chi}$ is calculated by its relationship with the mixture fraction variance $\tilde{\chi} = C_D \widetilde{\xi''^2}/\tau_\Delta$ [38] with C_D=4.0, $\widetilde{\xi''^2}$ the mixture fraction variance and τ_Δ the subgrid time scale. Here the statistical approach as in [39] is not used, because the an insufficient data distribution in any conditional bins affects not only the local values but also their neighbor values. Thus the strict requirement on the number of CFD cells in each flamelet zone as in [39] can be alleviated. Finally, the chemistry is solved using the conditional variables as the inputs of rate expressions,

$$\frac{\partial Q_i}{\partial t} = \langle W_i(Y_i, T)|\eta\rangle \approx W_i(Q_i, Q_T) \tag{11}$$

where Q_T is the conditional temperature. Such a first-order closure [34] is achieved by a Taylor expansion of the Arrhenius formula to the second order around the conditional means of reactive scalars, then conditionally averaging the result and neglecting all the terms involving conditional variances and covariances.

The conditional temperature Q_T influences the reaction progress in each mixture fraction bin space represented by a set of conditional mass fractions or called local flamelet if using the concept of RIF [40]. In addition to solving the flamelet or conditional temperature equations, various algebraic models has been proposed, e.g. the enthalpy defect/excess model [41-49] and Conditional Source-term Estimation (CSE) [50-52]. Here, the conditional temperature is not solved from its flamelet equation, mainly to avoid the complex construction of sub-models in the mixture fraction space for various heat additions or sinks, such as the conditional viscous dissipation, the conditional radiation terms and the conditional wall heat loss.

Ignoring the enthalpy defect fluctuations ($H' \sim o(0)$) [48], and therefore the corresponding PDF distribution of $\langle H|\eta\rangle$ can be assumed to be a Dirac delta function centered on the local mean value of the enthalpy $\widetilde{H}$. then $\langle H|\eta\rangle$ can be estimated using an approach of historical statistics,

$$\langle H|\eta\rangle = \left\langle \widetilde{H}\middle|\tilde{\xi} = \eta\right\rangle = \frac{1}{n}\sum_{t_{n-i}}^{t_n} \left\langle \widetilde{H}\middle|\tilde{\xi} = \eta\right\rangle \tag{12}$$

where n is the number of sampling data points with the condition $\tilde{\xi} = \eta$. Generally, the time sampling window $\Delta t = t_n - t_{n-i}$ should not span too many time steps, in order to reflect the latest temperature field. A similar statistical approach to obtain conditional variables has been implemented for high-resolution LES modeling in [39], where

quantities required on the flamelet zone are computed by integrating over all CFD cells within it. The statistical approach is especially suitable for LES because the CFD mesh resolution is high enough to minimize the scalar variance, such that the Favre-mean variables approach the instantaneous values. In dynamic zone flamelet, the requirement that a flamelet zone must contain sufficient CFD cells to give a good approximation of the actual conditional means is not necessary, because the conditional bin in the η space without being populated by the sampling process can be temporally "frozen" when solving Eq. (5). In the next time step, if the conditional bin is populated with at least one sampling point, the solving can be continued from the frozen status. A fact in dynamic zone flamelet is that the distribution of conditional mean in a single zone may be "defected", i.e., the true values in some conditional bins are absent. The defected conditional mean distribution will not affect the conditional reaction progress because the current active conditional bins correspond exactly to the mixture fraction distribution in the zone. Actually, such a statistical enthalpy approach mimics the enthalpy defect/excess model [41, 42] but provides a more reasonable estimation of the enthalpy defect/excess status in each zone. After that, the conditional temperature can be calculated as a function of conditional enthalpy and conditional mass fractions $Q_T = f(\langle H|\eta\rangle, Q_i)$. The current historical statistics approach also significantly saves the computational cost in directly solving the conditional energy equation with numerous conditional sub-models needed to be included for real supersonic combustion cases.

The β-function PDF is used in this study because of its continuous shape for integration and the implication of δ-function in its expression. $P(\eta)$ is given as a function of the mean mixture fraction $\tilde{\xi}$ and its variance $\widetilde{\xi''^2}$. Favre mean equations for $\tilde{\xi}$ and $\widetilde{\xi''^2}$ are respectively solved from their governing equations [53]. The mean species mass fractions $\widetilde{Y_i}$ are recovered by PDF weighted integration,

$$\widetilde{Y_i} = \int Q_i P(\eta) d\eta \tag{13}$$

and then mean temperature $\tilde{T}$ is obtained given $\widetilde{H}$ and $\widetilde{Y_i}$. As seen, unlike the traditional coupling between CFD and CMC, only the information of conditional mass fraction is returned for the PDF integration, while the conditional temperature is used only to control the reaction progress in each conditional bin. The mean density and temperature are not obtained from the integration of their corresponding conditional values, but rather solved from their ownunconditional governing equations.

The derivation of dynamic zone flamelet model is similar with the original CMC model [34], but the governing equations are formulated in a zone conserved form. The final equation describes the evolution of conditional reaction status or local flamelet due to spatial transport, η-space diffusion and local chemical reactions within a zone. Although similar with the coarser CMC grid, the zone concept actually defines an ensemble of CFD cells thus conveniently enables an irregular zone shape and a dynamic zone division. Through the dynamic zone division based on mean mixture fraction field, the conditional fluctuation terms become negligible as their redistribution effect diminishes gradually when the zone division is finer than the η-space discretization. Following the definition of zone based conditional averages, the spatial transport of conditional variables or local flamelet is calculated as a surface integral across the boundary faces of irregular neighbor zones. The final equation is also significantly simplified by the conditional independence assumption of density and velocity as in [54], suggesting by their weak correlations with mixture fraction in supersonic flows. Based on the mapping relation between the zone conditional averages and the high-resolution CFD variables, a novel statistical approach is used to estimate the conditional enthalpy assuming negligible enthalpy defect fluctuations, which not only avoids the complex construction of variable conditional enthalpy excess/defect sub-models in supersonic combustion but also significantly alleviates the computational cost.

III. Case validation of DZFM

A. Experimental case

The dynamic zone flamelet model (DZFM) is then applied to model the GH_2/GO_2 jet flame in a single-element rocket combustor. The geometry of a single-element rocket engine and its shear coaxial injector are schematically shown in Figure 1. The supercritical combustion of gaseous oxygen and hydrogen of a shear-coaxial injector was experimentally studied by Marshall et al. [55]. In the experiment, gaseous oxygen stream co-flowed by gaseous hydrogen stream was injected at the same static pressure of 5.2 MPa, and the static temperatures of 711 K and 800 K respectively. The mass compositions are 94.5% O_2 and 5.5% H_2O for the oxygen stream, while 40.2% H_2 and 59.8% H_2O for the hydrogen stream. The inlet jet velocities for the oxygen and hydrogen streams are 150 m/s and 750 m/s, which correspond to the Mach numbers of 0.31 and 0.51 respectively. The Reynolds numbers (Re) estimated based on the inlet parameters of oxygen and hydrogen streams are 6×10^5 and 1.6×10^5. The inlet diameter of the oxygen injector is 5.26 mm, the annulus inner and outer diameters of the hydrogen injector are 6.3 mm and 7.49 mm. The oxygen injector has a small recess length of 0.43 mm. The length and diameter of the cylinder combustion chamber

are 337 mm and 38.1 mm respectively. All combustion gas exit from the nozzle with a throat of 8.17 mm in diameter. Coaxial thermocouples are embedded in the chamber wall to measure the temperature and heat flux. The measured wall temperature is used as the thermal boundary condition in the modeling to evaluate the wall heat flux.

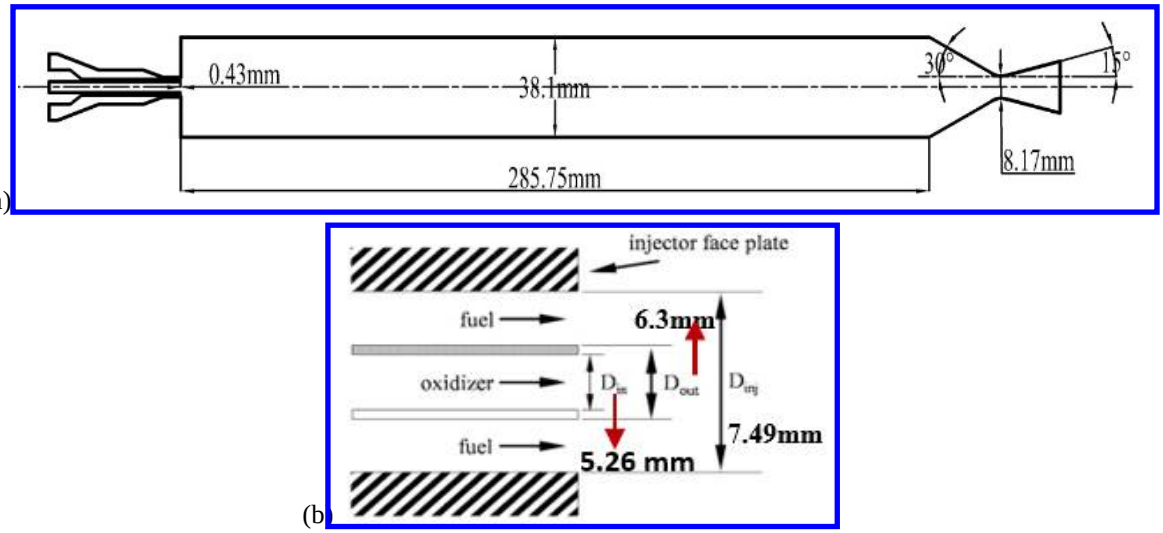

Figure 1. Schematic of (a) the rocket combustor and (b) its shear coaxial injector

B. Governing equations

The unsteady and three-dimensional Favre-averaged compressible reactive Navier-Stokes equations (rNSE) are solved for a set of conservative variables ($\bar{\rho}$, $\tilde{u}_i$, $\tilde{H}_t$, $\tilde{Y}_\alpha$),

$$\frac{\partial \bar{\rho}}{\partial t} + \frac{\partial \bar{\rho}\tilde{u}_j}{\partial x_j} = 0 \tag{14}$$

$$\frac{\partial \bar{\rho}\tilde{u}_i}{\partial t} + \frac{\partial \bar{\rho}\tilde{u}_j\tilde{u}_i}{\partial x_j} + \frac{\partial \bar{p}}{\partial x_i} - \frac{\partial \bar{\tau}_{ij}}{\partial x_j} = -\frac{\partial \tau_{ij}}{\partial x_j} \tag{15}$$

$$\frac{\partial \bar{\rho}\tilde{H}_t}{\partial t} + \frac{\partial \bar{\rho}\tilde{u}_j\tilde{H}_t}{\partial x_j} - \frac{\partial}{\partial x_j}\left(\bar{\rho}D_T\frac{\partial \tilde{H}_t}{\partial x_j} + \sum_{\alpha=1}^{L}\bar{\rho}D_\alpha\frac{\partial \tilde{Y}_\alpha}{\partial x_j}\tilde{H}_\alpha\right) - \frac{\partial \bar{p}}{\partial t} - \frac{\partial \tilde{u}_j\bar{\tau}_{ij}}{\partial x_j} = -\frac{\partial \Psi_{T,j}}{\partial x_j} \tag{16}$$

$$\frac{\partial \bar{\rho}\tilde{Y}_\alpha}{\partial t} + \frac{\partial \bar{\rho}\tilde{u}_j\tilde{Y}_\alpha}{\partial x_j} - \frac{\partial}{\partial x_j}\left(\bar{\rho}D_\alpha\frac{\partial \tilde{Y}_\alpha}{\partial x_j}\right) = -\frac{\partial \Psi_{\alpha,j}}{\partial x_j} + \bar{\omega}_\alpha \tag{17}$$

$$\bar{p} = \bar{\rho}R\tilde{T} \tag{18}$$

$$\tilde{H}_t = \tilde{H} + \frac{1}{2}\tilde{u}_i\tilde{u}_i = \tilde{H}^0 + \int_0^T C_p dT + \frac{1}{2}\tilde{u}_i\tilde{u}_i \tag{19}$$

Here the bar "-" and the tilde "~" represent averaged and Favre-averaged quantities respectively, t denotes the time, x_i is the Cartesian coordinate in direction i, $\bar{\rho}$ is the density, $\tilde{u}_i$ is the velocity component in x_i direction (spatial dimension i = 1, 2, 3), $\bar{p}$ is the pressure, $\bar{\tau}_{ij}$ is the viscous stress tensor, $\tilde{H}_t = \tilde{H} + 0.5\tilde{u}_i^2$ is the total absolute enthalpy obtained as the sum of the absolute enthalpy $\tilde{H}$ and the resolved kinetic energy, the absolute enthalpy $\tilde{H}$ is calculated as the sum of the formation enthalpy $\tilde{H}^0$ at standard reference state and the sensible enthalpy change from the reference temperature to T, $\tilde{Y}_\alpha$ is the mass fraction of species α (α = 1 , ..., L, with L the total species number), the specific heat C_p is a function of species concentrations and temperature, $\bar{\omega}_\alpha$ is the averaged mass production rate of chemical species α in the unit of $kg \cdot m^{-3} \cdot s^{-1}$, D_α is mixture-averaged mass diffusivity of species α, D_T is the thermal diffusivity, $\tilde{T}$ is the temperature, $R = R_u/W$ is the gas constant, $R_u = 8.314\, J \cdot mol^{-1} \cdot K^{-1}$ is the universal gas constant, $W = (\sum_{\alpha=1}^{L} Y_\alpha/W_\alpha)^{-1}$ is the molar weight of the multicomponent mixture. According to the Stokes's hypothesis which ignoring the bulk viscosity, the shear-stress tensor for a Newtonian fluid is calculated as:

$$\bar{\tau}_{ij} = \bar{\rho}\nu(\tilde{T})\left(2\tilde{S}_{ij} - \frac{2}{3}\delta_{ij}\tilde{S}_{kk}\right) \tag{20}$$

where ν is a temperature-dependent kinetic viscosity and the rate-of-strain tensor of the resolved scales is calculated as:

$$\tilde{S}_{ij} = \frac{1}{2}\left(\frac{\partial \tilde{u}_i}{\partial x_j} + \frac{\partial \tilde{u}_j}{\partial x_i}\right) \tag{21}$$

The thermodiffusion (Soret effect), barodiffusion and mass-driven diffusion of heat (Dufour effect) are ignored in Eqs. (16)-(17).

The turbulent Reynolds stresses (τ_{ij}) and turbulent fluxes ($\Psi_{T,j}$ and $\Psi_{\alpha,j}$) in Eqs. (14)-(19) are unclosed and both require specific modeling. The Reynolds stress, defined as $\tau_{ij} = \bar{\rho}\left(\widetilde{u_i u_j} - \tilde{u}_i \tilde{u}_j\right)$, is modeled by the Boussinesq eddy viscosity hypothesis, where the Reynolds stresses are also taken to be proportional to $\tilde{S}_{ij}$,

$$\tau_{ij} = \underbrace{\left(\tau_{ij} - \frac{1}{3}\delta_{ij}\tau_{kk}\right)}_{deviatoric} + \underbrace{\frac{1}{3}\delta_{ij}\tau_{kk}}_{isotropic} = -\bar{\rho}\nu_t\left(2\tilde{S}_{ij} - \frac{2}{3}\delta_{ij}\tilde{S}_{kk}\right) + \frac{2}{3}\delta_{ij}\bar{\rho}k_t \tag{22}$$

Here ν_t is the eddy viscosity given by the specified turbulence model, k_t is the unresolved turbulent kinetic energy. Because $\tau_{kk} = \gamma M a_t^2 \bar{p}$, with γ specific heat ratio, Ma_t unresolved Mach number and $\bar{p}$ filtered pressure, the isotropic term in Eq. (22) is expected to be small for weakly compressible flows and can be safely neglected when the turbulent Mach number of the flow is small. In this study, the Mach number inside the rocket combustor is mostly smaller than 0.3 except in the nozzle, thus the isotropic term is not solved.

The turbulent enthalpy flux term $\Psi_{T,j} = \bar{\rho}\left(\widetilde{u_j H_t} - \tilde{u}_j \tilde{H}_t\right)$ is modeled by the gradient diffusion assumption as

$$\Psi_{T,j} = -2\bar{\rho}\frac{\nu_t}{Pr_t}\frac{\partial \tilde{H}_t}{\partial x_j} \tag{23}$$

where Pr_t is the turbulent Prandtl number. The turbulent species diffusion term $\Psi_{\alpha,j} = \bar{\rho}\left(\widetilde{u_j Y_\alpha} - \tilde{u}_j \tilde{Y}_\alpha\right)$ is also modeled using the gradient diffusion assumption as

$$\Psi_{\alpha,j} = -2\bar{\rho}\frac{\nu_t}{Sc_t}\frac{\partial \tilde{Y}_\alpha}{\partial x_j} \tag{24}$$

where Sc_t is the turbulent Schmidt number. Unity Pr_t and Sc_t are used in this study.

C. Solver and numerical methods

In this study, Large Eddy Simulation (LES) modeling will be conducted by an OpenFOAM [56] based compressible reacting flow solver AstroFoam, which adopts the low-dissipative hybrid scheme [57] combining the dissipative Kurganov-Tadmor scheme [58] with the non-dissipative central scheme [59]. AstroFoam is extended from the standard compressible solver rhoCentrolFoam distributed with the open-source CFD package OpenFOAM V3.0.1 [56] mainly by adding the modules of species transportation and chemical reaction with realistic thermodynamics and transport properties. AstroFoam was firstly validated for various frozen flows, including the canonical shock tube problem, forward step flow, hypersonic flow over a biconic, and supersonic jets [60-67], and then applied to various scramjet combustor cases [68-75] to examine its accuracy and robustness in the modeling of complex supersonic combustion. The dynamic subgrid kinetic energy model (DKEM) [76] is used to model the subgrid-scale (SGS) turbulence effect. The effect of turbulent fluctuation on the turbulent reaction rate has been accounted for by the DZFM model assuming β-function PDF (probability density function) distributions of reacting scalars. In this study, the nonlinear inviscid convective fluxes are evaluated by using a second-order semi-discrete central Kurganov-Tadmor (KT) scheme [58] and the second-order central scheme in skew-symmetric form. A third-order spatial accuracy in reconstructing primitive convective fluxes at faces is achieved by the scale-selective discretization (SSD) scheme [77]. Temporal integration is advanced by the second-order Crank-Nicholson scheme [78].

As shown in Figure 2, the computational domain consists of the combustion chamber and the exhaust nozzle, while the external injector tube is excluded. The mesh consists of a total of 15.23 million unstructured cells, with a denser distribution clustering around the axis of the chamber. A near-wall inflation layer with a total thickness of 0.5 mm is distributed along the chamber wall to capture the ensuring the first near-wall cell located in a nondimensional wall distance y*<1. The domain is meshed by the Immersed Boundary (IB) CutCell method [79], which produces high-quality uniform hexahedral grid cells for most of the domain, while tetrahedron, wedge or pyramid cells filled only in large-curvature regions. The cell size smoothly transits from 0.25 mm near the chamber axis to 0.5 mm towards the outer region.

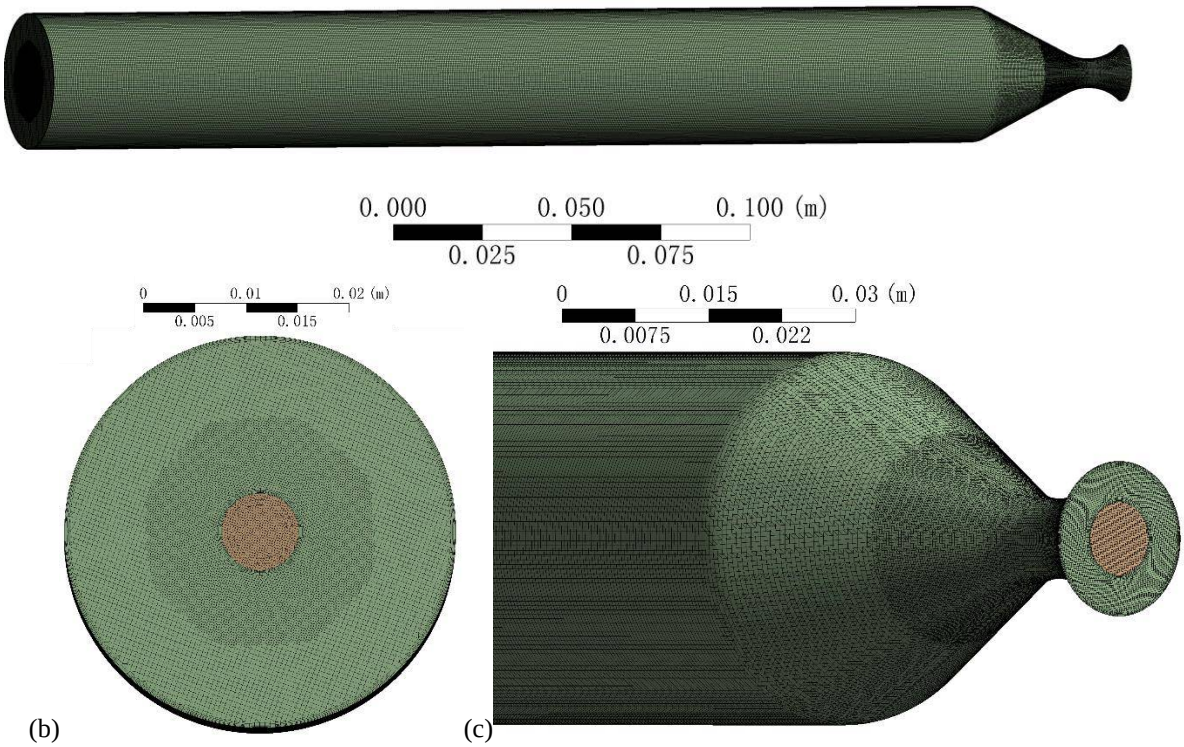

Figure 2. Mesh viewing from (a) the front side, (b) the injector bottom, and (c) the nozzle exit

The boundary conditions are set according to the experimental setup. The wall temperature are fixed as shown in Figure 3, where the axial temperature distribution along the radial wall of the combustion chamber using available experimental measurements, the bottom of the combustion chamber and the nozzle section are assumed to be fixed at 755 K and the nozzle temperature is assumed to be fixed at 510 K. At the nozzle exit, supersonic boundary conditions are applied. At all wall surfaces, no-slip conditions are used. The reference pressure for the current calculations was set at 5.2 MPa. And under this pressure, the bulk exit velocities of the oxidizer and fuel inlet are 150 m/s and 750m/s, respectively. The Reynolds numbers of the oxidizer and fuel inlet are 604,000 and 169,000, respectively.

A hydrogen/oxygen chemical mechanism with 9 species and 19 reversible reaction steps [80, 81], which has been validated over a wide pressure range (0.3-87 atm), is used to describe the combustion chemistry. Accurate fluid properties is crucial to reproduce the flow behaviors. Thermodynamic properties are obtained from the NIST-JANAF thermophysical database. Transport properties of the gas mixture, such as viscosity, thermal and mass diffusivities are calculated using the chemical kinetics package CHEMKIN-II [82] based on a CHEMKIN-format transport database. The mixture thermal diffusivity is calculated based on the conductivity and specific heat. Viscosity and thermal conductivity are averaged by the modified Wilke's law [83] and the combination averaging, respectively. Mass diffusivities are also mixture-averaged, and the mass conservation is achieved by setting nitrogen as the inert gas.

To reduce the computational cost near the wall and retain LES accuracy in the internal domain, Improved Delayed Detached Eddy Simulation (IDDES) [84] based on one-equation Spalart–Allmaras model [85] is employed. In IDDES, the near-wall region is resolved by traditional RANS modeling, and the outer flow region is treated with LES, with a smooth transition between the two regions. Near the wall, the IDDES length scale is determined by both the local cell sizes and the off-wall distance. A shielding function is applied to adjust the IDDES length scale to avoid the mismatch of the boundary layer edge due to excessively low subgrid viscosity. Such a treatment ensures that the boundary layer is fully covered by the RANS mode independent of the mesh distribution near the wall. The turbulence/chemistry interaction is modeled by the dynamic zone flamelet developed in this study.

The parallel computations are performed at the national supercomputer center in Tianjin (TH-1) using 140 CPU cores (Intel(R) Xeon(R) CPU E5-2690v4 with the base frequency of 2.60 GHz). The time step is limited both by a maximum Courant number of 0.3 and a user-specified maximum time step of 2×10^{-8} s. The flush through time (FTT) defined based on the length of the combustor flow-path length (0.337 m) and the inlet flow speed of the oxidizer stream (150 m/s) is $2.24\times10^{-3}\ s$, and was re-estimated to be 7 ms based on the flow depletion period. At least 2 FTTs (≈14 ms) are ensured for a meaningful data sampling and statistics.

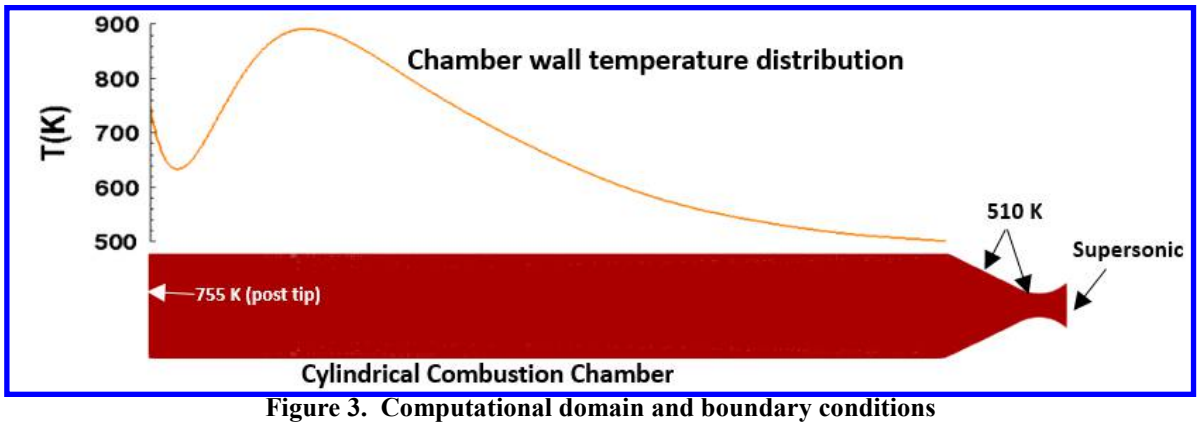

Figure 3. Computational domain and boundary conditions

IV. Results and discussion

Figure 4 compares the distributions of wall heat flux with the measurement and the literature data. As seen, the current numerical simulation denoted by the black solid line correctly predicts the heat flux profile, especially in the downstream region. While in the upper region, the calculated heat flux seems to be overpredicted in reference to the experimental measurement. While compared with other simulations, the Oefelein's result provides the best match with the experimental data over the entire length of the chamber, although with slight underprediction near the peak. This was expected since it has the highest fidelity with cell number 17 times more than this study. A further improvement in the modeling fidelity may help to improve the agreement, However, none of the modelings for this case have considered the radiative heat transfer, which should be considered since the gas temperature is as high as nearly 4000 K. If accounting for the contribution from radiation, the overpredicted heat flux in the front end should be compensated.

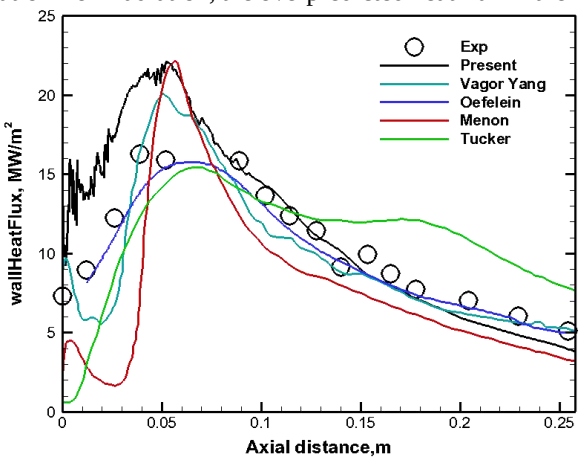

Figure. 4 Present numerical predictions of heat flux profiles compared to experimental data and other simulaitons

The flow-through time that is simply estimated from the inlet velocity is inaccurate for that the streamwise flow speed may vary significantly. For the examined case, the flow-through time (FTT) defined based on the length of the combustor flow-path length (0.337 m) and the inlet flow speed of the oxidizer stream (150 m/s) is 2.24 ms. The depletion period of a certain species is used to re-estimate the flow through time. In the modeling, the combustion chamber was firstly filled with the oxidizer composition and temperature as the initial condition. As can be seen from Figure 5, a FTT of 7 ms was defined when initial oxidizer has been completely depleted. As seen, the flow through time defined by the flow depletion is significantly larger than that defined by the inlet flow speed. Modeling was first proceeded for two flow-through times to wash out the initial residuals. Time-averaging and flow statistics are then collected for two flow-through times.

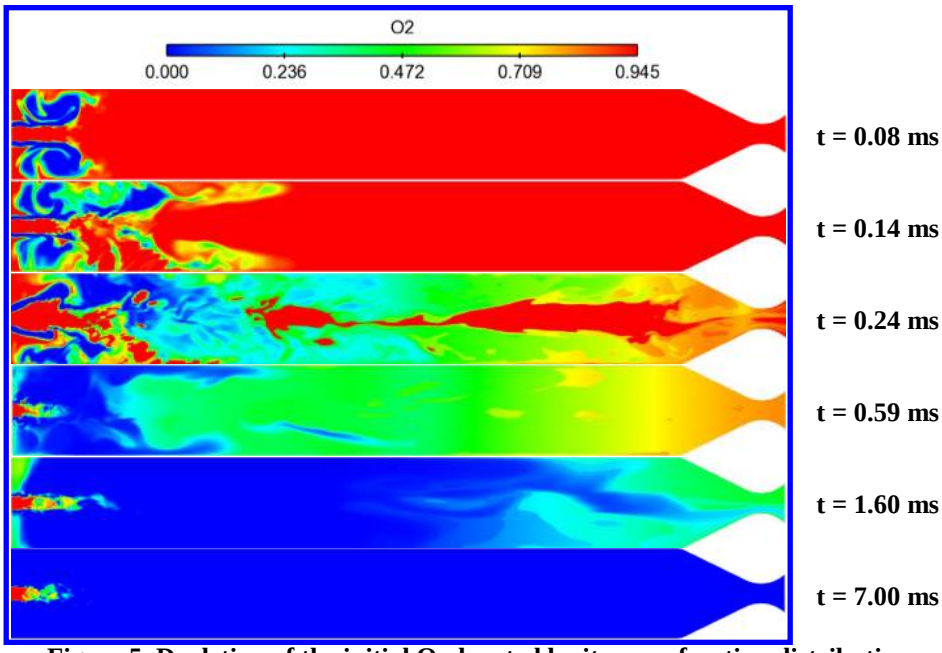

Figure 5. Depletion of the initial O_2 denoted by its mass fraction distribution

Figure 6 shows instantaneous fields of temperature and mass fractions of H_2, O_2, OH, and H_2O. The chamber pressure is lower than both the initial pressure of fuel and oxidizer, thus expansion occurs near the injectors. Due to the larger velocity difference between the fuel and the oxidizer jets, strong shear layers occur. Both the expansion and the shear stress speed up the breakup of the jets within a short distance from the injector exit. The arising large-scale flow structures promote the complete mixing between reactants, which produce a flame temperature higher than 3500 K. No obvious plume structures can be observed since $6D_{inj}$. Besides the jet regions, the surrounding gas temperature gradually increases as the streamwise distance increases. The final temperature near the nozzle reaches around 3000 K, which causes stringent requirement on the wall cooling facility. Due to the fixed wall temperature, a thick thermal boundary layer is formed to insulate the wall from the hot combustion gas. The distribution of OH indicates that the main reaction region persists until $10D_{inj}$. Due to the spatial convection of flamelet information from the upstream to the downstream, a weak multi-layer structure can be observed in the OH distribution, indicating that they are calculated based on different flamelet. An improvement in the zone division would help to smooth the species difference across the zones. However, no obvious multi-layer structures were observed for other species, such as H_2, O_2, and H_2O. This suggests that those intermediate species with highly transient behavior are more sensitive to the zone division, as their concentrations vary significantly with the local conditions.

(a)

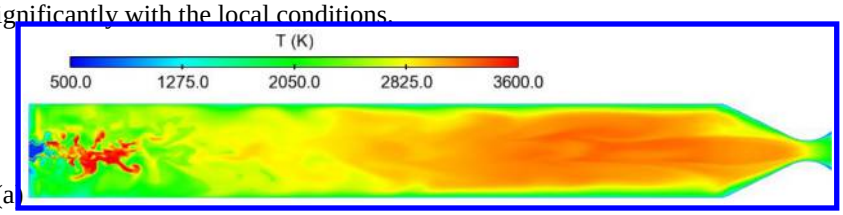

(b)

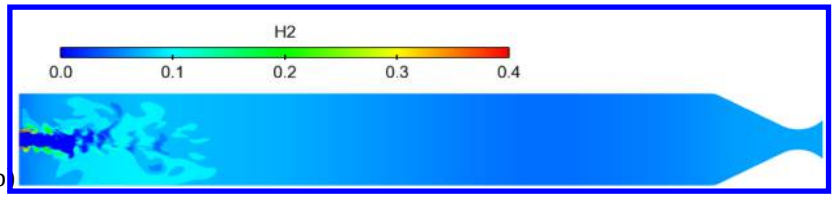

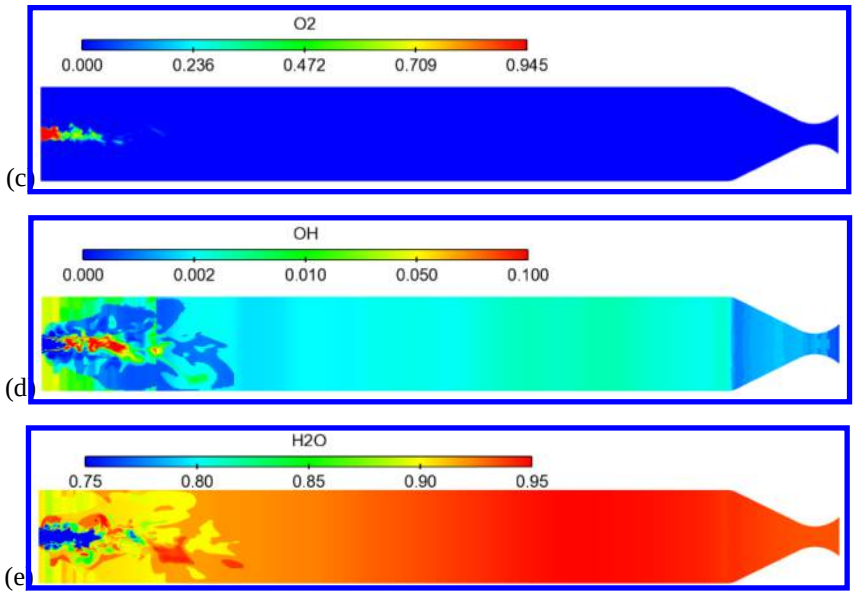

Figure 6. Instantaneous fields of (a) temperature and mass fractions of (b) H_2, (c) O_2, (d) OH, and (e) H_2O.

Figure 7 shows the time-averaged fields of temperature and mass fractions of H_2, O_2, OH, and H_2O over two FTTs. A high-temperature region is formed corresponding to the main jet breakup region. Besides the jet, the highest gas temperature occurs slightly downstream of the middle of the chamber. The oxygen jet penetrates only a small distance of around $5D_{inj}$ into the combustion chamber before it mixes with the oxidizer and the surrounding combustion gas. Due to its low molecule weight and correspondingly lower jet momentum, the penetration depth of the hydrogen jet is even smaller. Thermal expansion in the radial direction of the hydrogen coflow can be observed. As indicated by the OH distribution, in addition to the main reaction zone in the oxidizer jet wake, there is also intense reactions attached to the chamber bottom. Due to the lack of oxygen there, the OH is indeed produced from the pyrolysis reaction of H_2O, which takes a large proportion of 59.8% in the hydrogen stream. From Figure 7(d), the mass fraction of H_2O is lower near the bottom and increases gradually with the axial distance, which is an evidence of the fact that the OH near the bottom is produced from the pyrolysis reaction of H_2O rather than from the combustion reactions between H_2 and O_2. Due to the lack of oxygen, the pyrolyzed OH have less chance to participate into the combustion reactions, but the recirculation zone will transport part of those intermediate species into the downstream reaction zone and thus it acts as the role of radical farming [86] for the flame ignition. In the downstream of the recirculation zone, the chamber is filled with a high concentration of water vapor, which as a polar gas has a rather high absorption coefficient and thus radiative heat transfer need to be accounted for in the future study.

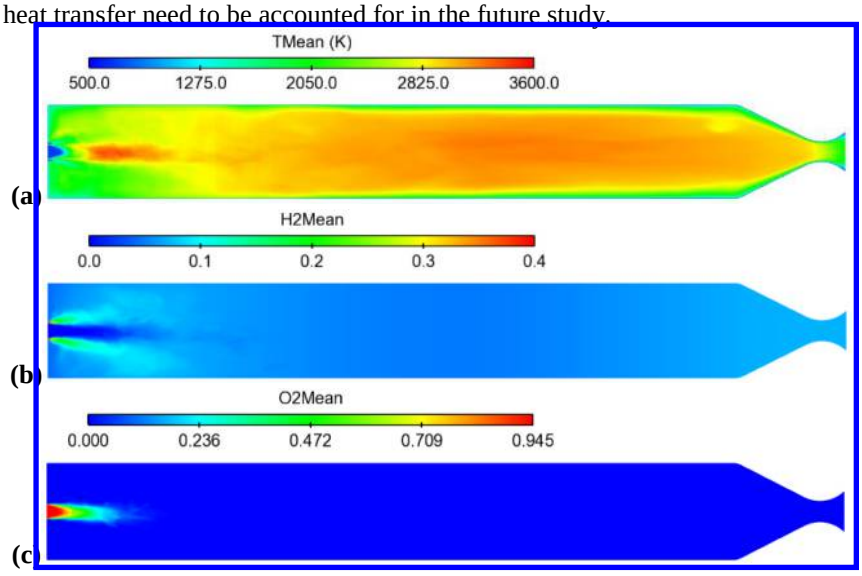

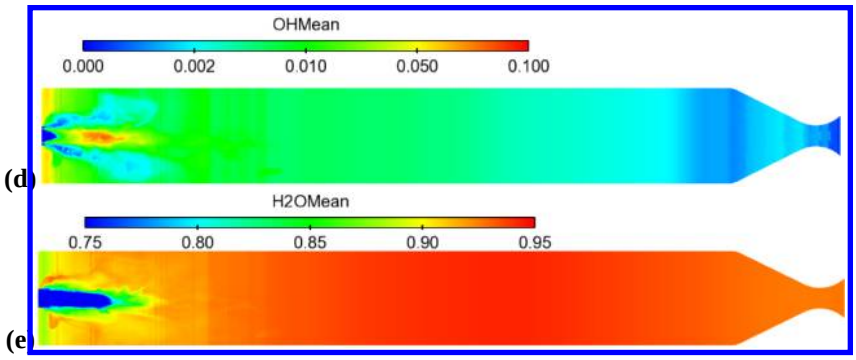

Figure 7. Time-averaged fields of temperature and mass fractions of H_2, O_2, OH, and H_2O

Figure 8 shows the mean streamlines overlaid on the temperature field in the near field of the injector. The recirculation zone structure, in terms of size, shape, and location, has a major impact on the redistribution of species and reaction zones, and thus significantly affects the wall heat flux on the front chamber part. Compared with the predictions for the current examined case reported in the literature, only the results of Huo [87] and Menon [88] show similar vortex shape, while the others exhibit significant differences. The largest recirculation zone in the current prediction is similar to the predictions of Huo [87] and Menon [88] in the scale and the location of vortex center. Due to the entrainment of the recirculation zone, part of the fuel stream is carried to the chamber bottom, and the continue reactions result in a rich OH concentration there as shown in Figure 7(d).

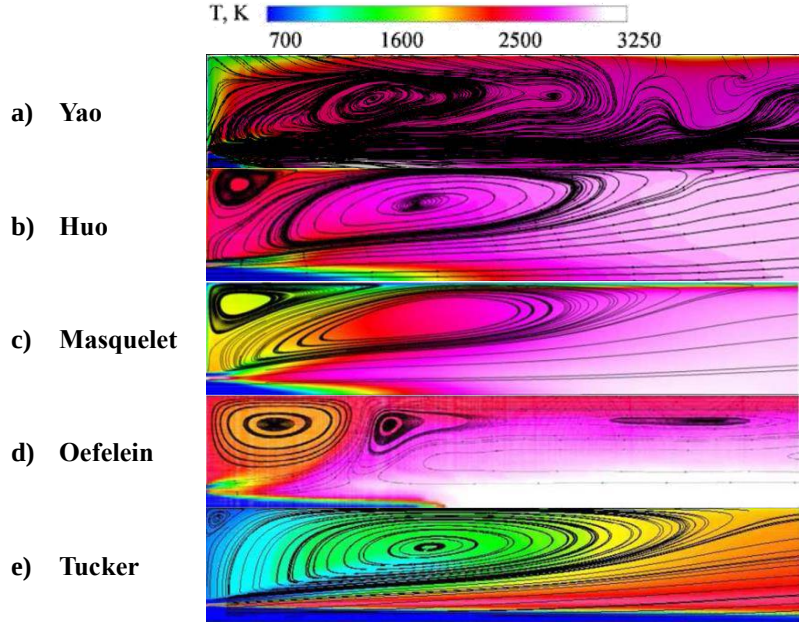

Figure 8. Comparison of time-averaged streamlines overlaid on temperature given by (a) the present study, (b) Huo et al. [87], (c) Masquelet and Menon [88], (d) Oefelein [89], and (e)Tucker et al. [89]

Figure 9 compared the time-averaged temperature fields for each calculation. As see, the flame structures vary significantly from one case to another case, especially for the height of the unburned oxidizer jet and the radial expansion of the flame. The difference in the major recirculation zones certainly has an important impact on the flame shape. The current modeling has the smallest height for the unburnt oxidizer jet, indicating that the mixing between the hydrogen and oxygen is quicker and a premixed flame is formed in the downstream. The modeling given by Tucker et al. [89] shows the highest height of the unburnt oxidizer jet, which almost penetrates into the middle of the chamber. The flame expands to reach the lateral wall at a downstream distance of around $10D_{inj}$ in the modelings by Huo et al. [87] and Masquelet et al. [88], while expands slowly to reach the lateral wall at around $22D_{inj}$ in the modeling by Tucker et al. [89]. In the current modeling and the one by Oefelein [89], the flame itself is away from the lateral wall,

although the hot combustion gas fills in the chamber. In the cases of Masquelet et al. [88] and Oefelein [89] as well as the current cases, there is a region with a relatively low temperature near the chamber bottom and surrounding the injectors, which may be caused by the endothermic pyrolysis reactions of H_2O into OH and H.

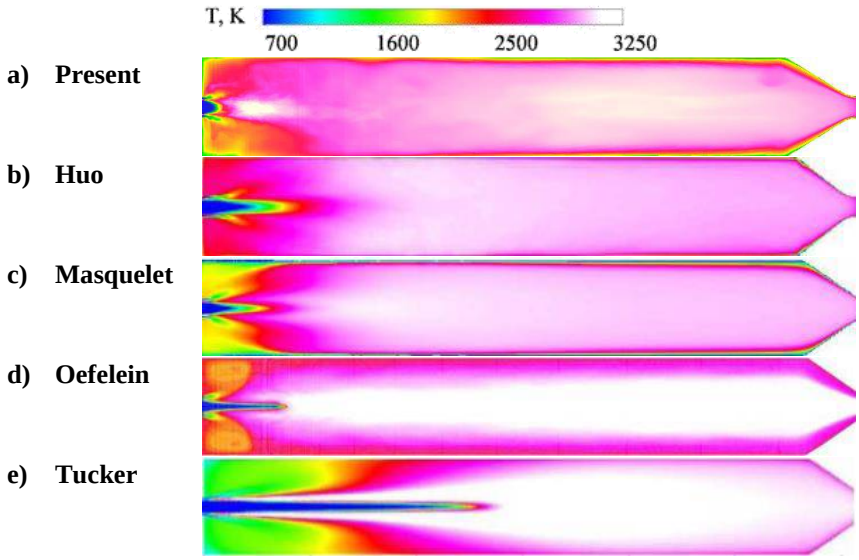

Figure 9. Comparison of time-averaged temperature fields given by (a) the present study, (b) Huo et al. [87], (c) Masquelet and Menon [88], (d) Oefelein [89], and (e)Tucker et al. [89]

Figure 10 compares the radial profiles of temperature from the present study and the literature at the axial locations of 0.0125, 0.025, 0.05, and 0.15 m downstream of the injector. From Figure 8, the first three probes located inside the recirculation region, while the last one (x=0.15m) is in the downstream. The current predictions are generally in accordance with those reported in the literature. At x=0.0125 m and 0.025 m, the temperature on the axis has a significant rise compared with the others, indicating that the combustion reactions start earlier in this study; while away from the axis, the current predictions are in good agreement with those given by Masquelet et al. [88] at al. At the downstream locations of x=0.05 and 0.15 m, the current predictions are similar to that given by Masquelet et al. [88] in the whole profile and to that given by Lian et al. [90] in the radial location away from the axis.

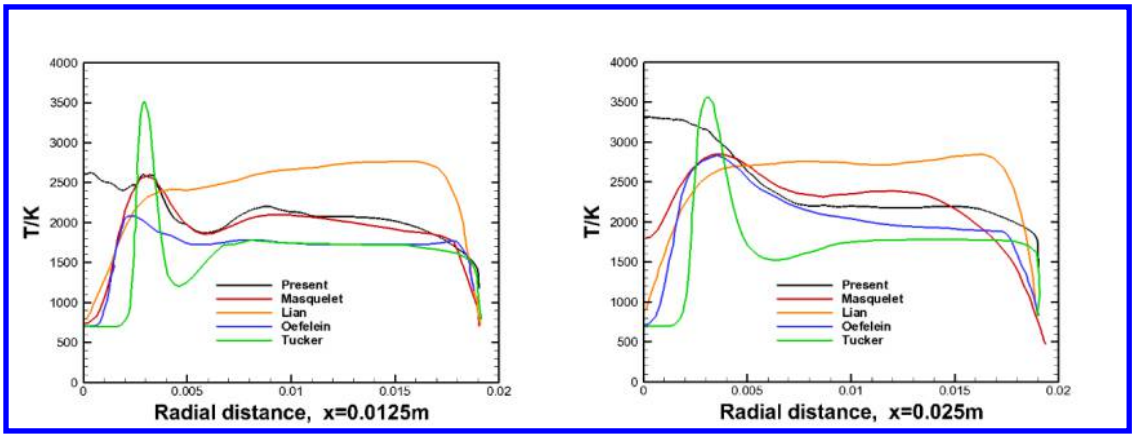

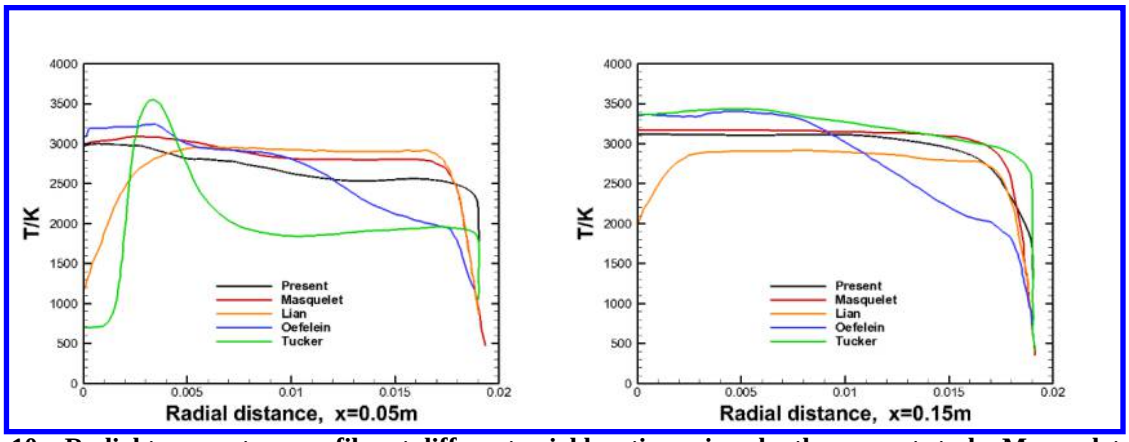

Figure 10. Radial temperature profiles at different axial locations given by the present study, Masquelet et al. [88], Lian et al. [90], Oefelein [89], and Tucker et al. [89]

Figure 11 shows the radial profiles of hydrogen mass fraction at different axial locations predicted by the present study and from the literature. At x=0.0125 and 0.025 m, the current predictions are in good agreements with that predicted by Masquelet et al. [88] and also comparable with that predicted by Lian et al. [90]. At the downstream locations of x=0.05 and 0.15 m, the hydrogen distribution approaches a homogeneous mixing status, as in the case of Masquelet et al. [88].

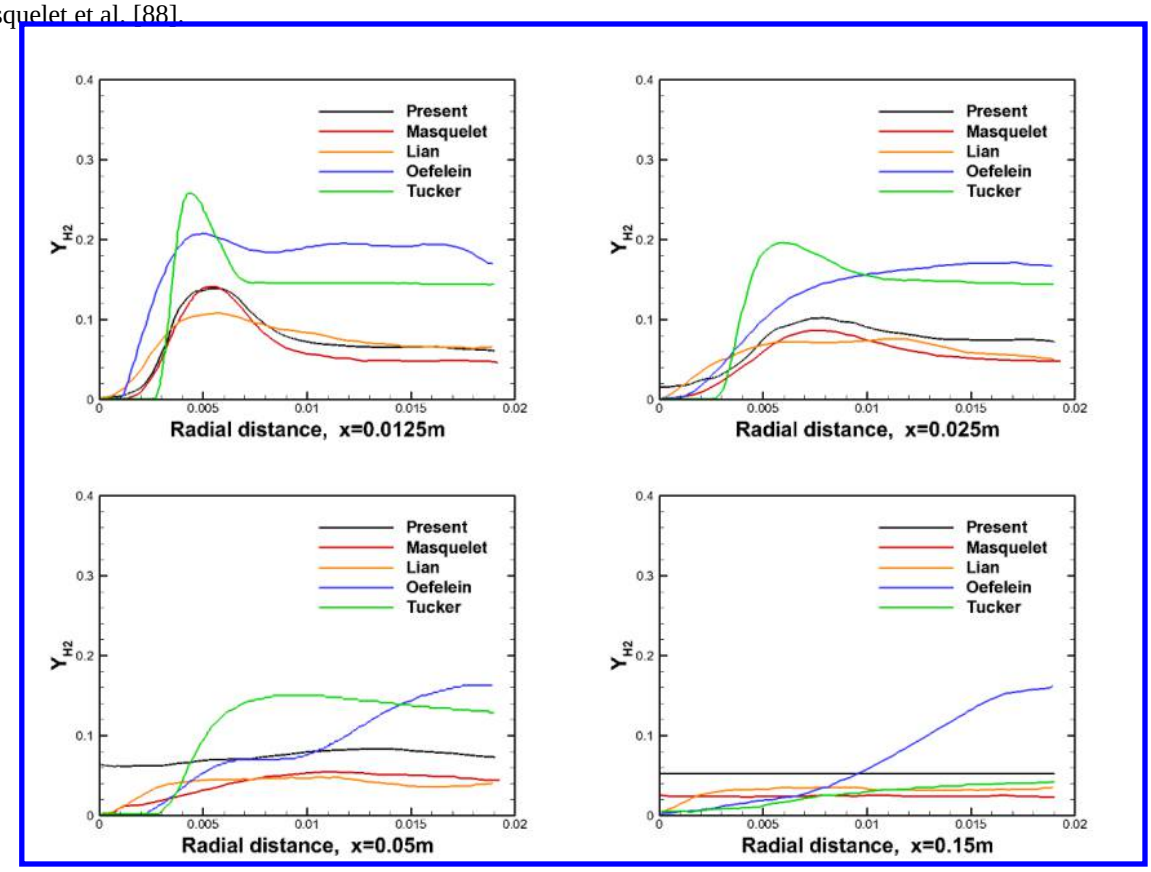

Figure 11. Radial profiles of hydrogen mass fraction at different axial locations given by the present study, Masquelet et al. [88], Lian et al. [90], Oefelein [89], and Tucker et al. [89]

Figure 12 shows the distribution of flamelet zones at different heights. The flamelet zone is divided according to a short-time averaged mixture fraction field. As seen, the flamelet zones vary with the axial height since the mixture fraction distribution varies. Each zone corresponds to a narrow mixture fraction space. Note that if the narrow mixture

fraction space does not correspond to any subset of the averaged mixture fraction field, the current flamelet zone will be "frozen" temporally. For example, at x=0.005, the mixture fraction concentrates around the axis, thus only a few numbers of flamelet zones corresponding to the extreme of fuel-rich and oxygen-rich conditions are activated. As the jet moves downstream, the mixture fraction distribution spans in the radial direction, thus more flamelet zones corresponding to a wide range of mixture fraction are activated. In the further downstream, the fuel-rich mixture fraction range vanishes due to the dispersion, thus only those flamelet zones corresponding to fuel-lean conditions are activated. The flamelet information is transferred from the higher mixture fraction range in the upstream to the lower mixture fraction in the downstream. The diffusion in the mixture fraction space mimics the diffusion of reacting parcels in the physical space. The diffusion of radicals across the mixture fraction space can also ignite the mixture in the surrounding mixture fraction bins, which mimics the ignition process in the physical space. The zone is in irregular shape and contains a random number of cells. The zone division is updated every a fixed number of time steps to keep up with the time-variant mixture fraction fields. Note that the zone does not need to be continuous, but can be composed of several isolated "islands" as long as their local mixture fraction falls into to the mixture fraction bin that is allocated to the flamelet zone.

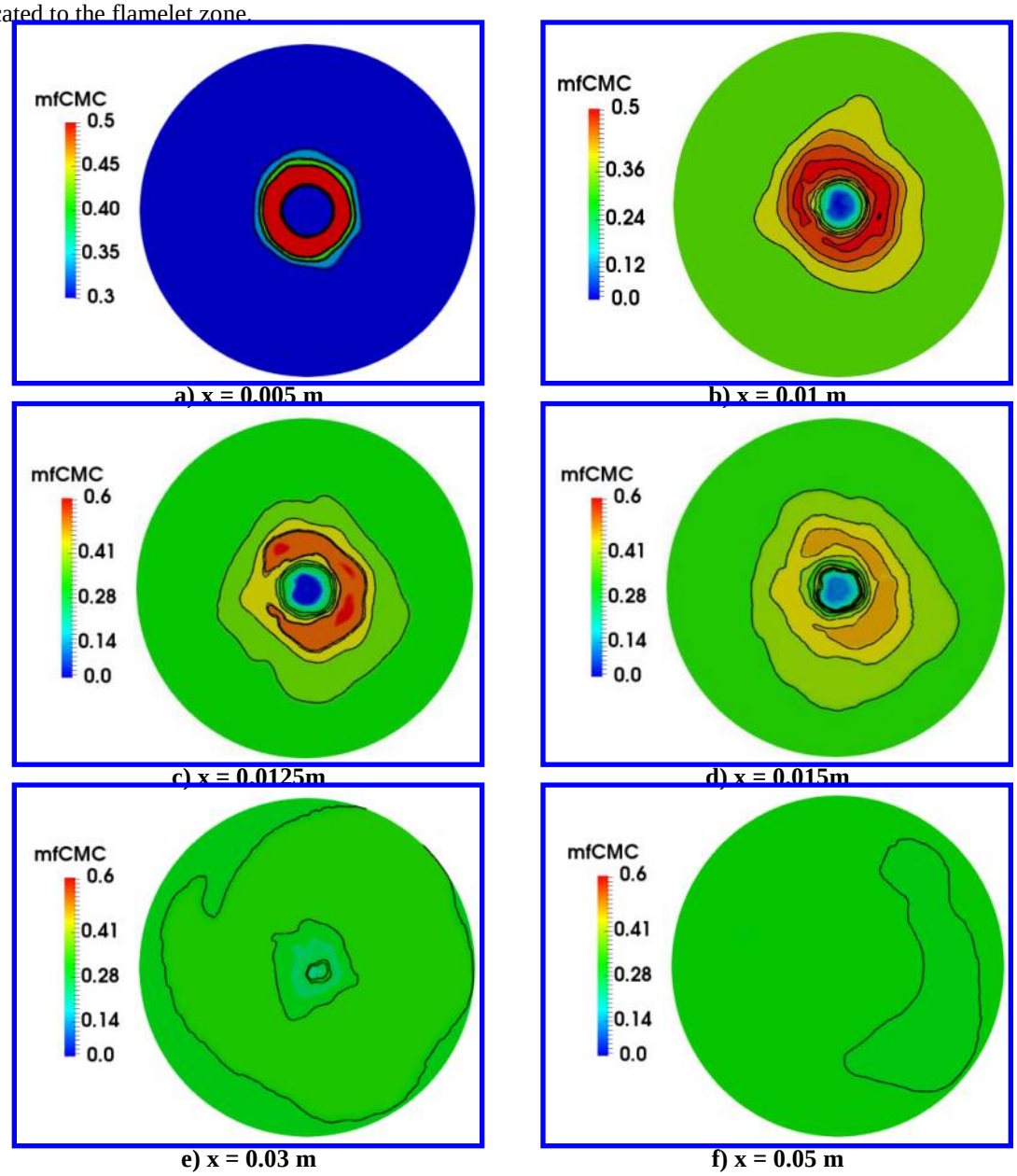

Figure 12. Zone divisions according to the mixture fraction fields at different axial heights

Figure 13 shows the temperature and composition information extracted from the flamelets at different axial heights. As seen, with the increasing of axial heights, the oxidizer (O_2) concentration decreases while the product concentration (H_2O) increases, indicating that the reaction progress proceeds gradually with the flow residence time. As the combustion reactions approach equilibrium, the mass fractions of intermediate species, such as H, OH, and HO_2 decrease as well. The high OH concentration in the flamelets at low HABs confirms the high OH concentration near the chamber bottom in Figure 7 (d). In Figure 13, the flamelets corresponding to the bin of stoichiometric mixture fraction are extracted. At a further downstream, the mixture fraction all drop to values below the stoichiometric mixture fraction due to the dispersion of fuel stream, thus the flamelet above the maximum local mixture fraction will be frozen, as the flamelet at HAB (height above the burner)=12 mm. The flamelet at HAB=12 mm maintains the unreacted pure mixing status, and this flamelet will not be used in the PDF integration. Note that the temperature status in the flamelet is not used in the PDF integration to obtain the mean temperature, only the composition in the flamelet is used to calculate the mean species. The energy equation is then solved directly based on the mean species to better account for the non-adiabatic effect.

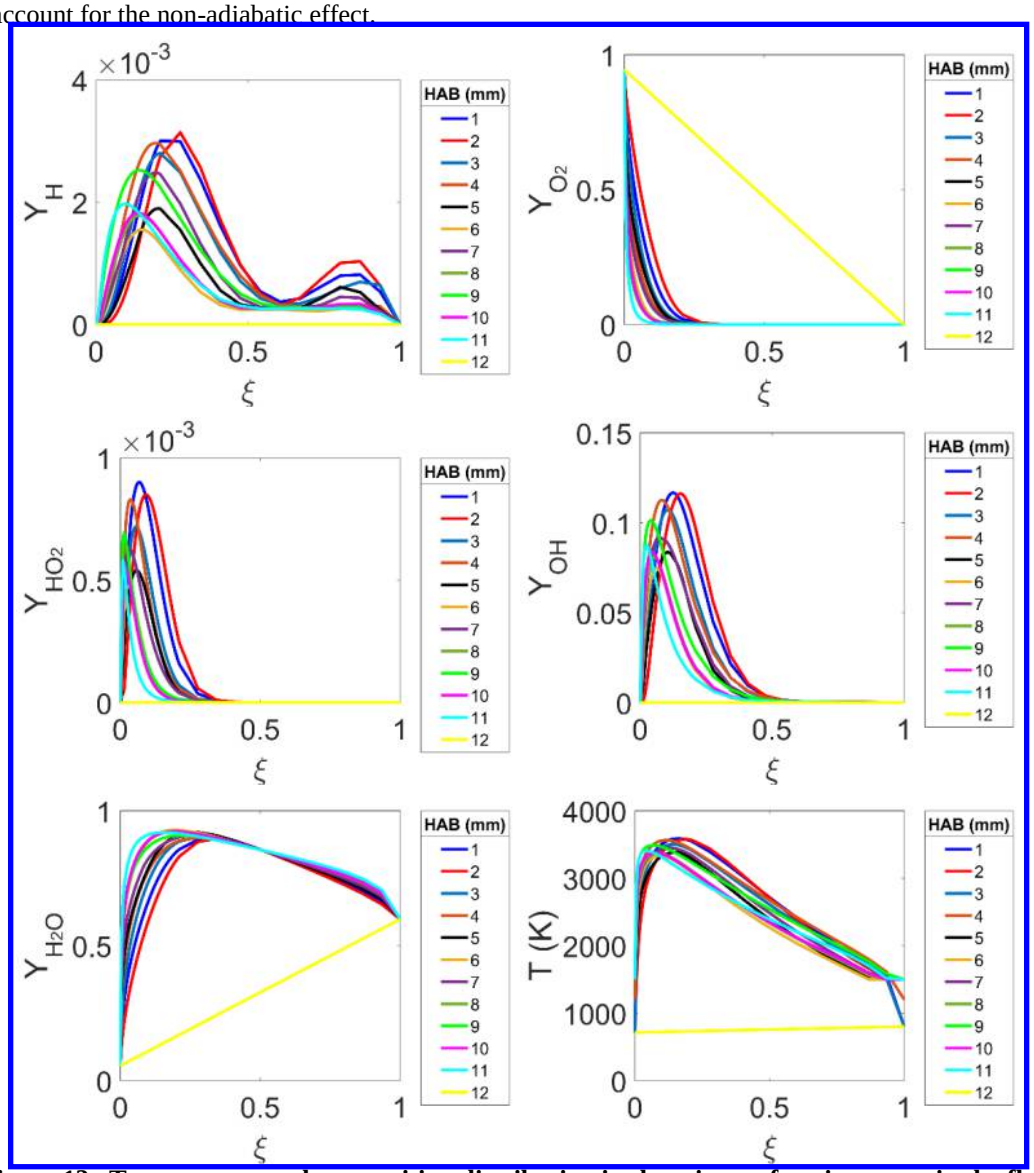

Figure 13. Temperature and composition distribution in the mixture fraction space in the flamlets extracted at different axial heights.

Figure 14 and 15 show the evolution of H_2O mass fraction of H_2O and temperature in the flamelets with a time interval of 2×10^{-5} s. As seen, the species mass fraction varies not only with the axial height but also with the time, indicating that the current model has the capability of characterizing the transient chemistry status, which is especially

useful for unsteady combustion modeling by large eddy simulation. Since the flamelets are extracted during the quasi-steady stage, thus the flamelet variables fluctuate periodically around the same level. The representative temperature is not used in the PDF integration, but it is a good indicator for the reaction progress. The peak temperature shifts from the fuel-rich side towards the stoichiometric mixture fraction because the chemical dissociation weakens as the combustion reactions approach the equilibrium. Due also to the unsteadiness caused by the recirculation zone, the flamelet temperature varies more noticeable at low HABs, while the flamelet variables at the downstream locations remain nearly unchanged with the time.

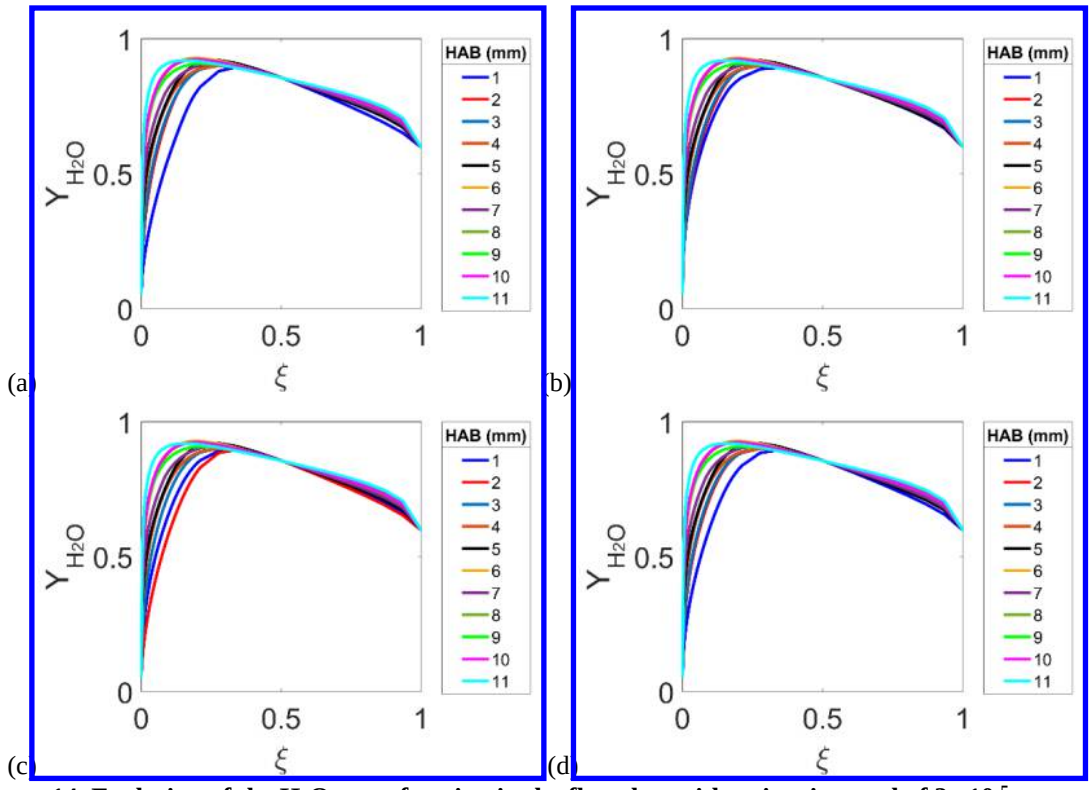

Figure 14. Evolution of the H_2O mass fraction in the flamelets with a time interval of 2×10^{-5} s

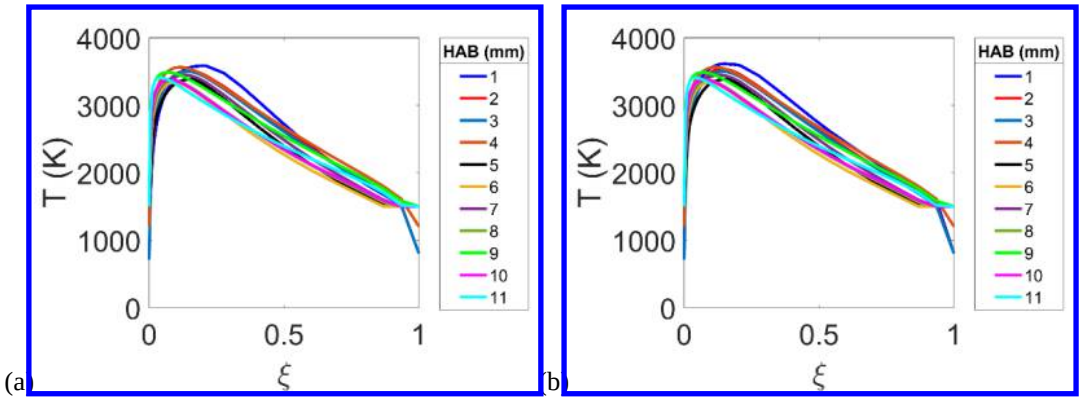

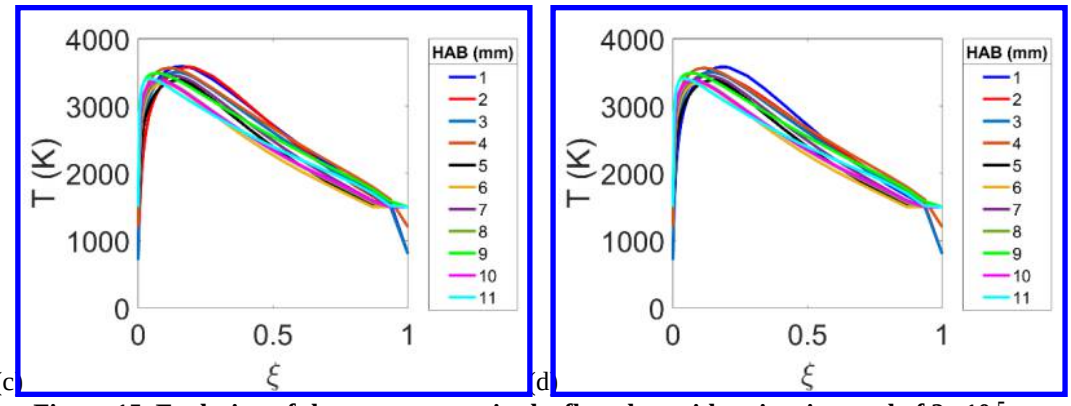

(c) (d)

Figure 15. Evolution of the temperature in the flamelets with a time interval of 2×10^{-5} s

Conclusions

In this study, a dynamic zone flamelet model (DZFM) has been developed. The model divides the whole computational domain into different zones according to both the physical coordinate and time-variant mixture fraction fields. The evolution of conditional variables or local flamelet within a zone due to convective transport, molecular diffusion, and local chemistry is described by a governing equation, which is derived through redefining the conditional average within each zone. In highly compressible supersonic flows, the density, temperature, and velocity do not correlate with the mixture fraction any more, thus only the species mass fraction in each flamelet is used in the PDF integration. The flamelet temperature equation is not solved, but the conditional temperature is obtained based on a statistical method within each flamelet zone. Based on such a dynamic zone division method, each zone is in irregular shape and contains a random number of CFD cells. Each flamelet zone corresponds to a narrow bin in the mixture faction space, and if none of the CFD cells have the mixture fraction value within the current mixture fraction bin, the current flamelet zone will be deactivated temporally.

The model is then applied to a GH_2/GO_2 rocket combustor based on an Improved Delayed Detached Eddy Simulation (IDDES) framework. The predicted wall heat flux, mean temperature and mean hydrogen concentration are generally comparable with the available experimental measurement and the previous predictions in the literature. Compared with traditional flamelet model, the current model gives a more accurate description of the reaction progress as the jet flows downstream through representing the local chemistry status using a local flamelet within each zone. A total of 20557 flamelet zones are used, with 61 in the mixture fraction space and 337 along the axial direction in the physical space. As the zone shrinks, the number of sampling data points reduces, then Q_i approaches Y_i and $Q_i' \to 0$. Through further refining the flamelet zones, a higher-fidelity modeling of the reacting fields can be achieved since the local chemistry status has been more accurately described. The evolution of flamelet variables with the axial height and the time shows that the current model has the capability of characterizing the transient chemistry status in the framework of large eddy simulation.

Acknowledgments

The project was supported by the Training Program of the Major Research Plan of the National Natural Science Foundation of China (Grant No. 91641110), the Open founding of National Key Laboratory of Science and Technology on Aero-Engine Aero-Thermodynamics (Grant No. 6142702180307), and LHD Innovative Foundation (Grant No. LHD2018JS01). The authors are also grateful to the National Supercomputer Center in Tianjin for providing the computational resource.

References

1. Imren, A., and Haworth, D. C., "On the Merits of Extrapolation-Based Stiff Ode Solvers for Combustion CFD," *Combustion and Flame*, Vol. 174, 2016, pp. 1-15. doi: 10.1016/j.combustflame.2016.09.018
2. Lu, T., and Law, C. K., "Toward Accommodating Realistic Fuel Chemistry in Large-Scale Computations," *Progress in Energy and Combustion Science*, Vol. 35, No. 2, 2009, pp. 192-215. doi: 10.1016/j.pecs.2008.10.002
3. Contino, F., Jeanmart, H., Lucchini, T., and D'Errico, G., "Coupling of in Situ Adaptive Tabulation and Dynamic Adaptive Chemistry: An Effective Method for Solving Combustion in Engine Simulations," *Proceedings of the Combustion Institute*, Vol. 33, No. 2, 2011, pp. 3057-3064. doi: 10.1016/j.proci.2010.08.002
4. Liang, L., Stevens, J. G., and Farrell, J. T., "A Dynamic Adaptive Chemistry Scheme for Reactive Flow Computations," *Proceedings of the Combustion Institute*, Vol. 32, No. 1, 2009, pp. 527-534. doi: 10.1016/j.proci.2008.05.073

5. Pepiot-Desjardins, P., and H.Pitsch, "An Efficient Error-Propagation-Based Reduction Method for Large Chemical Kinetic Mechanisms," *Combustion and Flame,* Vol. 154, 2008, pp. 67-81. doi: 10.1016/j.combustflame.2007.10.020
6. Lu, T., and Law, C. K., "Linear Time Reduction of Large Kinetic Mechanisms with Directed Relation Graph: N-Heptane and Iso-Octane," *Combustion and Flame,* Vol. 144, No. 1-2, 2006, pp. 24-36. doi: 10.1016/j.combustflame.2005.02.015
7. Pope, S. B., "Computationally Efficient Implementation of Combustion Chemistry Using in Situ Adaptive Tabulation," *Combustion Theory and Modeling,* Vol. 1, No. 1, 1997, pp. 41-63. doi: 10.1080/713665229
8. Yang, B., and Pope, S. B., "Treating Chemistry in Combustion with Detailed Mechanisms - in Situ Adaptive Tabulation in Principal Directions - Premixed Combustion," *Combustion and Flame,* Vol. 112, 1998, pp. 85-112. doi: 10.1016/S0010-2180(97)81759-2
9. Jangi, M., and Bai, X.-S., "Multidimensional Chemistry Coordinate Mapping Approach for Combustion Modelling with Finite-Rate Chemistry," *Combustion Theory and Modelling,* Vol. 16, No. 6, 2012, pp. 1109-1132. doi: 10.1080/13647830.2012.713518
10. Baris, S., and Suresh, M., "Artificial Neural Networks Based Chemistry-Mixing Subgrid Model for LES," *47th AIAA Aerospace Sciences Meeting including The New Horizons Forum and Aerospace Exposition*, Orlando, Florida, 5-8 January, 2009. doi: 10.2514/6.2009-241
11. Baris, S., and Suresh, M., "Representation of Chemical Kinetics by Artificial Neural Networks for Large Eddy Simulations," *43rd Aiaa/Asme/Sae/Asee Joint Propulsion Conference & Exhibit*. American Institute of Aeronautics and Astronautics, 2007.doi: 10.2514/6.2007-5635
12. Rajat, K., Vaidyanathan, S., and Suresh, M., "Towards Engineering LES of Reacting Flows:Artificial Neural Networks for Efficient Kinetics Modeling," *41st Aerospace Sciences Meeting and Exhibit*, Reno, Nevada, 6-9 January, 2003. doi: 10.2514/6.2003-311
13. Chen, J. Y., Blasco, J. A., Fueyo, N., and Dopazo, C., "An Economical Strategy for Storage of Chemical Kinetics: Fitting in Situ Adaptive Tabulation with Artificial Neural Networks," *Proceedings of the Combustion Institute,* Vol. 28, No. 1, 2000, pp. 115-121. doi: 10.1016/s0082-0784(00)80202-7
14. Niemeyer, K. E., and Sung, C.-J., "Accelerating Moderately Stiff Chemical Kinetics in Reactive-Flow Simulations Using Gpus," *Journal of Computational Physics,* Vol. 256, 2014, pp. 854-871. doi: 10.1016/j.jcp.2013.09.025
15. Peters, N., "Laminar Diffusion Flamelet Models in Non-Premixed Turbulent Combustion," *Progress in Energy and Combustion Science,* Vol. 10, 1984, pp. 319-339.doi: 10.1016/0360-1285(84)90114-X
16. Golovitchev, V. I., and jarnicki, R., "Numerical Modeling of High Temperature Air "Flameless" Combustion," *The 4th International Symposium on High Temperature Air Combustion and Gasification*, Rome, Italy, 26-30 November, 2001.
17. Golovitchev, V. I., Nordin, N., Jarnicki, R., and Chomiak, J., "3-D Diesel Spray Simulations Using a New Detailed Chemistry Turbulent Combustion Model." SAE Technical Paper 2000-01-18912000. doi: 10.4271/2000-01-1891
18. Magnussen, B. F., "On the Structure of Turbulence and a Generalized Eddy Dissipation Concept for Chemical Reaction in Turbulent Flow," *19th American Institute of Aeronautics and Astronautics Aerospace Science Meeting*, St. Louis, Missouri, January 12-15, 1981.doi: 10.2514/6.1981-42
19. Magnussen, B. F., "The Eddy Dissipation Concept: A Bridge between Science and Technology," *ECCOMAS Thematic Conference on Computational Combustion*, Lisbon, Portugal, 21-24 June, 2005.
20. Yao, W., and Fan, X., "Development of Zone Flamelet Model for Scramjet Combustor Modeling ". AIAA 2017-22772017. doi: 10.2514/6.2017-2277
21. Triantafyllidis, A., Mastorakos, E., and Eggels, R. L. G. M., "Large Eddy Simulations of Forced Ignition of a Non-Premixed Bluff-Body Methane Flame with Conditional Moment Closure," *Combustion and Flame,* Vol. 156, No. 12, 2009, pp. 2328-2345. doi: 10.1016/j.combustflame.2009.05.005
22. Milford, A., and Devaud, C. B., "Investigation of an Inhomogeneous Turbulent Mixing Model for Conditional Moment Closure Applied to Autoignition," *Combustion and Flame*, Vol. 157, No. 8, 2010, pp. 1467-1483. doi: 10.1016/j.combustflame.2010.05.001
23. Milford, A. E., and Devaud, C. B., "Application of an Inhomogeneous Turbulent Mixing Model in Conditional Moment Closure for Autoignition," *6th Mediterranean Combustion Symposium*, Ajaccio, Corsica, France, June 7-11, 2009.
24. Richardson, E. S., Chakraborty, N., and Mastorakos, E., "Analysis of Direct Numerical Simulations of Ignition Fronts in Turbulent Non-Premixed Flames in the Context of Conditional Moment Closure," *Proceedings of the Combustion Institute,* Vol. 31, No. 1, 2007, pp. 1683-1690. doi: 10.1016/j.proci.2006.07.221
25. Kronenburg, A., and Papoutsakis, A. E., "Conditional Moment Closure Modeling of Extinction and Re-Ignition in Turbulent Non-Premixed Flames," *Proceedings of the Combustion Institute,* Vol. 30, No. 1, 2005, pp. 759-766. doi: 10.1016/j.proci.2004.08.235
26. Sreedhara, S., and Lakshmisha, K. N., "Assessment of Conditional Moment Closure Models of Turbulent Autoignition Using Dns Data," *Proceedings of the Combustion Institute*, Vol. 29, 2002, pp. 2069-2077.doi: 10.1016/S1540-7489(02)80252-8
27. Kim, W. T., and Huh, K. Y., "Numerical Simulation of Spray Autoignition by the First-Order Conditional Moment Closure Model," *Proceedings of the Combustion Institute*, Vol. 29, 2002, pp. 569-576.doi: 10.1016/S1540-7489(02)80073-6
28. Sreedhara, S., and Lakshmisha, K. N., "Direct Numerical Simulation of Autoignition in a Non-Premixed, Turbulent Medium," *Proceeding of the Combustion Institute,* Vol. 28, 2000, pp. 25-34.doi: 10.1016/S0082-0784(00)80191-5

29. Ingenito, A., and Bruno, C., "Physics and Regimes of Supersonic Combustion," *AIAA Journal*, Vol. 48, No. 3, 2010, pp. 515-525. doi: 10.2514/1.43652
30. O'Brien, E. E., and Jiang, T.-L., "The Conditional Dissipation Rate of an Initially Binary Scalar in Homogeneous Turbulence," *Physics of Fluids*, Vol. 3, No. 12, 1991, pp. 3121-3123.doi: 10.1016/S0082-0784(00)80191-5
31. Girimaji, S. S., "On the Modeling of Scalar Diffusion in Isotropic Turbulence," *Physics of Fluids*, Vol. 4, No. 11, 1992, pp. 2529-2537.doi: 10.1063/1.858440
32. Kronenburg, A., Bilger, R. W., and Kent, J. H., "Computation of Conditional Average Scalar Dissipation in Turbulent Jet Diffusion Flames," *Flow, Turbulence and Combustion*, Vol. 64, 2000, pp. 145-159.doi: 10.1023/A:1009912404132
33. Sreedhara, S., Lee, Y., Huh, K. Y., and Ahn, D. H., "Comparison of Submodels for Conditional Velocity and Scalar Dissipation in Cmc Simulation of Piloted Jet and Bluff-Body Flames," *Combustion and Flame*, Vol. 152, No. 1-2, 2008, pp. 282-286. doi: 10.1016/j.combustflame.2007.08.008
34. Klimenkoa, A. Y., and Bilger, R. W., "Conditional Momen Closure for Turbulent Combustion," *Progress in Energy and Combustion Science*, Vol. 25, 1999, pp. 595-687. doi: 10.1016/S0360-1285(99)00006-4
35. Bilger, R. W., "Conditional Moment Closure for Turbulent Reacting Flow," *Physics of Fluids*, Vol. 5, No. 2, 1993, pp. 436-444.doi: 10.1063/1.858867
36. Kronenburg, A., and Bilger, R. W., "Modelling of Differential Diffusion Effects in Nonpremixed Nonreacting Turbulent Flow," *Physics of Fluids*, Vol. 9, No. 5, 1997, pp. 1435-1447.doi: 10.1080/00102200108907825
37. Navarro-Martinez, S., Kronenburg, A., and Mare, F. D., "Conditional Moment Closure for Large Eddy Simulations," *Flow Turbulence and Combustion*, Vol. 75, 2005, pp. 245-274.doi: 10.1007/s10494-005-8580-7
38. Pera, C., Reveillon, J., Vervisch, L., and Domingo, P., "Modeling Subgrid Scale Mixture Fraction Variance in LES of Evaporating Spray," *Combustion and Flame*, Vol. 146, 2006, pp. 635-648.doi: 10.1016/j.combustflame.2006.07.003
39. Thornber, B., Bilger, R. W., Masri, A. R., and Hawkes, E. R., "An Algorithm for LES of Premixed Compressible Flows Using the Conditional Moment Closure Model," *Journal of Computational Physics*, Vol. 230, No. 20, 2011, pp. 7687-7705. doi: 10.1016/j.jcp.2011.06.024
40. Pitsch, H., Wan, Y. P., and Peters, N., "Numerical Investigation of Soot Formation and Oxidation under Diesel Engine Conditions," 1995. doi: 10.4271/952357
41. Cleary, M., and Kent, J., "Modelling of Species in Hood Fires by Conditional Moment Closure," *Combustion and Flame*, Vol. 143, No. 4, 2005, pp. 357-368. doi: 10.1016/j.combustflame.2005.08.013
42. Young, K. J., and Moss, J. B., "Modeling Sooting Turbulent Jet Flames Using an Extended Flamelet Technique," Combustion Science and Technology, Vol. 105, 1995, pp. 33-53. doi: 10.1080/00102209508907738
43. Brookes, S. J., and Moss, J. B., "Predictions of Soot and Thermal Radiation Properties in Confined Trubulent Jet Diffusion Flames," Combustion and Flame, Vol. 116, 1999, pp. 486-503. doi: 10.1016/S0010-2180(98)00056-X
44. Kennedy, I. M., Kollmannt, W., and Ghen, J. Y., "Predictions of Soot in Laminar Diffusion Flames," AIAA Journal, Vol. 29, No. 9, 1991, pp. 1452-1457. doi: 10.2514/3.10759
45. Bai, X. S., Balthasar, M., Mauss, F., and Fuchs, L., "Detailed Soot Modeling in Turbulent Jet Diffusion Flames," Proceeding of combustion institute, Vol. 27, 1998, pp. 1623-1630. doi: 10.1016/S0082-0784(98)80572-9
46. Louis, J. J. J., Kok, J. B. W., and Klein, S. A., "Modeling and Measurements of a 16-Kw Turbulent Nonadiabatic Syngas Diffusion Flame in a Cooled Cylindrical Combustion Chamber," Combustion and Flame, Vol. 125, 2001, pp. 1012-1031. doi: 10.1016/S0010-2180(01)00223-1
47. Kim, G., Kang, S., Kim, Y., and Lee, K.-S., "Conditional Moment Closure Modeling for a Three-Dimensional Turbulent Non-Premixed Syngas Flame with a Cooling Wall," Energy and Fuels, Vol. 22, 2008, pp. 3639-3648. doi: 10.1021/ef800182c
48. Cuoci, A., Frassoldati, A., Faravelli, T., and Ranzi, E., "Kinetic Modeling of Soot Formation in Turbulent Nonpremixed Flames," *Environmental Engineering Science*, Vol. 25, No. 10, 2008, pp. 1407-1422. doi: 10.1089/ees.2007.0193
49. Yao, W., Zhang, J., Nadjai, A., Beji, T., and Delichatsios, M., "Development and Validation of a Global Soot Model in Turbulent Jet Flames," *Combustion Science and Technology*, Vol. 184, No. 5, 2012, pp. 717-733. doi: 10.1080/00102202.2012.661495
50. Wang, M., Huang, J., and Bushe, W. K., "Simulation of a Turbulent Non-Premixed Flame Using Conditional Source-Term Estimation with Trajectory Generated Low-Dimensional Manifold," *Proceedings of the Combustion Institute*, Vol. 31, No. 2, 2007, pp. 1701-1709. doi: 10.1016/j.proci.2006.07.104
51. Bushea, W. K., and Steiner, H., "Conditional Moment Closure for Large Eddy Simulation of Nonpremixed Turbulent Reacting Flow," *Physics of Fluids*, Vol. 11, No. 7, 1999, pp. 1896-1906. doi: 10.1063/1.870052
52. Bushe, W. K., and Salehi, M. M., "Conditional Source-Term Estimation a Tool for Combustion Simulation in the Gas Turbine Context," University of British Columbia 2010.
53. Jones, W. P., and Whitelaw, J. H., "Calculation Methods for Reacting Turbulent Flows: A Review," Combustion and Flame, Vol. 48, 1982, pp. 1-26. doi: 10.1016/0010-2180(82)90112-2
54. Smith, N. S. A., Bilger, R. W., and Chen, J.-Y., "Modeling of Nonpremixed Hydrogen Jet Flames Using a Conditional Moment Closure Method," Twenty-Fourth Symposium (International) on Combustion, The Combustion Institute, pp. 263-269, 1992. doi: 0.1016/S0082-0784(06)80035-4
55. Marshall, W. M., Pal, S., Woodward, R. D., and Santoro, R. J., "Benchmark Wall Heat Flux Data for a Go2/Gh2 Single Element Combustor." AIAA 2005-3572, July 10-13 2005. doi: 10.2514/6.2005-3572

56. Weller, H. G., Tabor, G., Jasak, H., and Fureby, C., "A Tensorial Approach to CFD Using Object Oriented Techniques," *Computers in Physics*, Vol. 12, No. 6, 1997, pp. 620-631. doi: 10.1063/1.168744
57. Lee, Y., Yao, W., and Fan, X., "Low-Dissipative Hybrid Compressible Solver Designed for Large Eddy Simulation of Supersonic Turbulent Flows," *AIAA Journal*, Vol. 56, No. 8, 2018, pp. 3086-3096. doi: 10.2514/1.J056404
58. Kurganov, A., and Tadmor, E., "New High-Resolution Central Schemes for Nonlinear Conservation Laws and Convection–Diffusion Equations," *Journal of Computational Physics*, Vol. 160, No. 1, 2000, pp. 241-282. doi: 10.1006/jcph.2000.6459
59. Pirozzoli, S., "Generalized Conservative Approximations of Split Convective Derivative Operators," *Journal of Computational Physics*, Vol. 229, No. 19, 2010, pp. 7180-7190. doi: 10.1016/j.jcp.2010.06.006
60. Wu, K., Li, X., Yao, W., and Fan, X., "Three-Dimensional Numerical Study of the Acoustic Properties of a Highly Underexpanded Jet." AIAA 2015-3572, 6-9 July 2015. doi: 10.2514/6.2015-3572
61. Li, X., Wu, K., Yao, W., and Fan, X., "A Comparative Study of Highly Underexpanded Nitrogen and Hydrogen Jets Using Large Eddy Simulation." AIAA 2015-3573, 6-9 July 2015. doi: 10.2514/6.2015-3573
62. Greenshields, C. J., Weller, H. G., Gasparini, L., and Reese, J. M., "Implementation of Semi-Discrete, Non-Staggered Central Schemes in a Colocated, Polyhedral, Finite Volume Framework, for High-Speed Viscous Flows," *International Journal for Numerical Methods in Fluids*, Vol. 38, No. 2, 2009, pp. 139-161. doi: 10.1002/fld.2069
63. Li, X., Yao, W., and Fan, X., "Large-Eddy Simulation of Time Evolution and Instability of Highly Underexpanded Sonic Jets," *AIAA Journal*, Vol. 54, No. 10, 2016, pp. 3191-3211. doi: 10.2514/1.J054689
64. Li, X., Zhou, R., Yao, W., and Fan, X., "Flow Characteristic of Highly Underexpanded Jets from Various Nozzle Geometries," *Applied Thermal Engineering*, Vol. 125, 2017, pp. 240-253. doi: 10.1016/j.applthermaleng.2017.07.002
65. Li, X., Fan, E., Yao, W., and Fan, X., "Numerical Investigation of Characteristic Frequency Excited Highly Underexpanded Jets," *Aerospace Science and Technology*, Vol. 63, 2017, pp. 304-316. doi: 10.1016/j.ast.2017.01.005
66. Lee, Y., Yao, W., and Fan, X., "A Low-Dissipation Solver Based on Openfoam Designed for Large Eddy Simulation in Compressible Flows." AIAA 2017-2444, 6-9 March 2017. doi: 10.2514/6.2017-2444
67. Li, X., Wu, K., Yao, W., and Fan, X., "A Comparative Study of Highly Underexpanded Nitrogen and Hydrogen Jets Using Large Eddy Simulation," *International Journal of Hydrogen Energy*, Vol. 41, No. 9, 2015, pp. 5151-5161. doi: 10.1016/j.ijhydene.2016.01.120
68. Yao, W., Wang, J., Lu, Y., Li, X., and Fan, X., "Full-Scale Detached Eddy Simulation of Kerosene Fueled Scramjet Combustor Based on Skeletal Mechanism." AIAA 2015-3579, 6-9 July 2015. doi: 10.2514/6.2015-3579
69. Wu, K., Zhang, P., Yao, W., and Fan, X., "Numerical Investigation on Flame Stabilization in Dlr Hydrogen Supersonic Combustor with Strut Injection," *Combustion Science and Technology*, Vol. 189, No. 12, 2017, pp. 2154-2179. doi: 10.1080/00102202.2017.1365847
70. Yao, W., Lu, Y., Li, X., Wang, J., and Fan, X., "Improved Delayed Detached Eddy Simulation of a High-Ma Active-Cooled Scramjet Combustor Based on Skeletal Kerosene Mechanism." AIAA-2016-4761, 25-27 July 2016. doi: 10.2514/6.2016-4761
71. Yao, W., Yuan, Y., Li, X., Wang, J., Wu, K., and Fan, X., "Comparative Study of Elliptic and Round Scramjet Combustors Fueled by RP-3," *Journal of Propulsion and Power*, Vol. 34, No. 3, 2018, pp. 772-786. doi: arc.aiaa.org/doi/abs/10.2514/1.B36721
72. Wu, K., Yao, W., and Fan, X., "Development and Fidelity Evaluation of a Skeletal Ethylene Mechanism under Scramjet-Relevant Conditions," *Energy & Fuels*, Vol. 31, No. 12, 2017, pp. 14296-14305. doi: 10.1021/acs.energyfuels.7b03033
73. Yao, W., Lu, Y., Wu, K., Wang, J., and Fan, X., "Modeling Analysis of an Actively-Cooled Scramjet Combustor under Different Kerosene/Air Ratios," *Journal of Propulsion and Power*, Vol. 34, No. 4, 2018, pp. 975-991. doi: doi.org/10.2514/1.B36866
74. Yao, W., Wu, K., and Fan, X., "Influences of Domain Symmetry on Supersonic Combustion Modeling," *Journal of Propulsion and Power*, Vol. 35, No. 2, 2019, pp. 451-465. doi: 10.2514/1.B37227
75. Yao, W., Lu, Y., Wu, K., Wang, J., and Fan, X., "Modeling Analysis of an Actively Cooled Scramjet Combustor under Different Kerosene/Air Ratios," *Journal of Propulsion and Power*, Vol. 34, No. 4, 2018, pp. 975-991. doi: 10.2514/1.B36866
76. Won-Wook, K., and Suresh, M., "A New Dynamic One-Equation Subgrid-Scale Model for Large Eddy Simulations," *33rd Aerospace Sciences Meeting and Exhibit*, Reno, NV, January 9-12, 1995. doi: 10.2514/6.1995-356
77. Vuorinen, V., Larmi, M., Schlatter, P., Fuchs, L., and Boersma, B. J., "A Low-Dissipative, Scale-Selective Discretization Scheme for the Navier–Stokes Equations," *Computers & Fluids*, Vol. 70, 2012, pp. 195-205. doi: 10.1016/j.compfluid.2012.09.022
78. Baba-Ahmadi, M. H., and Tabor, G., "Inlet Conditions for LES Using Mapping and Feedback Control," *Computers & Fluids*, Vol. 38, No. 6, 2009, pp. 1299-1311. doi: 10.1016/j.compfluid.2009.02.001
79. Clarke, D. K., Hassan, H. A., and Salas, M. D., "Euler Calculations for Multielement Airfoils Using Cartesian Grids," *AIAA Journal*, Vol. 24, No. 3, 1986, pp. 353-358. doi: 10.2514/3.9273
80. Burke, M. P., Chaos, M., Ju, Y., Dryer, F. L., and Klippenstein, S. J., "Comprehensive H2/O2 Kinetic Model for High-Pressure Combustion," *International Journal of Chemical Kinetics*, Vol. 44, No. 7, 2012, pp. 444-474. doi: 10.1002/kin.20603
81. Li, J., Zhao, Z., Kazakov, A., and Dryer, F. L., "An Updated Comprehensive Kinetic Model of Hydrogen Combustion," *International Journal of Chemical Kinetics*, Vol. 36, No. 10, 2004, pp. 566-575. doi: 10.1002/kin.20026

82. Kee, R. J., Rupley, F. M., and Miller, J. A., "Chemkin-II: A Fortran Chemical Kinetics Package for the Analysis of Gas-Phase Chemical Kinetics," Sandia National Laboratories, Technical Report SAND89-8009B, Sandia, 1 September 1989. doi: 10.2172/481621
83. Bird, R. B., Stewart, W. E., and Lightfoot, E. N., "Viscosity and the Mechanisms of Momentum Transport," *Transport Phenomena (2nd Edition)*. John Wiley & Sons, New York, 2002, p. 27.
84. Shur, M. L., Spalart, P. R., Strelets, M. K., and Travin, A. K., "A Hybrid RANS-LES Approach with Delayed-Des and Wall-Modelled LES Capabilities," *International Journal of Heat and Fluid Flow,* Vol. 29, 2008, pp. 1638-1649. doi: 10.1016/j.ijheatfluidflow.2008.07.0
85. Spalart, P. R., and Allmaras, S. R., "A One-Equation Turbulence Model for Aerodynamic Flows." AIAA-92-0439, 6-9 January 1992. doi: 10.2514/6.1992-439
86. McGuire, J. R., Boyce, R. R., and Mudford, N. R., "Radical-Farm Ignition Processes in Two-Dimensional Supersonic Combustion," *Journal of Propulsion and Power,* Vol. 24, No. 6, 2008, pp. 1248-1257. doi: 10.2514/1.35562
87. Huo, H., and Yang, V., "Large-Eddy Simulation of Supercritical Combustion: Model Validation against Gaseous H2–O2 Injector," *Journal of Propulsion and Power,* Vol. 33, No. 5, 2017, pp. 1272-1284. doi: 10.2514/1.B36368
88. Masquelet, M., and Menon, S., "Large-Eddy Simulation of Flame-Turbulence Interactions in a Shear Coaxial Injector," *Journal of Propulsion and Power,* Vol. 26, No. 5, 2011, pp. 924-935. doi: 10.2514/1.48023
89. Tucker, P. K., Menon, S., Merkle, C. L., Oefelein, J. C., and Yang, V., "Validation of High-Fidelity CFD Simulations for Rocket Injector Design." AIAA 2008-5226, 21-23 July 2008. doi: 10.2514/6.2008-5226
90. Lian, C., Merkle, C. L., and Xia, G., "Flowfield Initialization and Approach to Stationary Conditions in Unsteady Combustion Simulations," *Computer and Fluids,* Vol. 39, 2010, pp. 310–323. doi: 10.1016/j.compfluid.2009.09.009